AGU PUBLICATIONS

Paleoceanography

RESEARCH ARTICLE
10.1002/2014PA002681

Key Points:
- Productivity controls sedimentary opal, organic carbon, and trace Ag and Cd
- Oxygenation/redox controls stratigraphy and sedimentary Re and Mo contents
- Guaymas Basin records differ from NE Pacific sites

Supporting Information:
- Readme
- Table S1

Correspondence to:
A. S. Chang,
asm_chang@yahoo.com

Citation:
Chang, A. S., L. Pichevin, T. F. Pedersen, V. Gray, and R. Ganeshram (2015), New insights into productivity and redox-controlled trace element (Ag, Cd, Re, and Mo) accumulation in a 55 kyr long sediment record from Guaymas Basin, Gulf of California, *Paleoceanography*, *30*, 77–94, doi:10.1002/2014PA002681.

Received 9 JUN 2014
Accepted 12 JAN 2015
Accepted article online 16 JAN 2015
Published online 19 FEB 2015

New insights into productivity and redox-controlled trace element (Ag, Cd, Re, and Mo) accumulation in a 55 kyr long sediment record from Guaymas Basin, Gulf of California

Alice S. Chang[1,2], Laetitia Pichevin[3], Thomas F. Pedersen[1], Victoria Gray[1], and Raja Ganeshram[3]

[1]School of Earth and Ocean Sciences, University of Victoria, Victoria, British Columbia, Canada, [2]Now at Department of Forest and Conservation Sciences, University of British Columbia, Vancouver, British Columbia, Canada, [3]School of Geosciences, Grant Institute, University of Edinburgh, Edinburgh, UK

Abstract A high-resolution, 55 kyr long record of chalcophile and redox-sensitive trace element accumulation (Ag, Cd, Re, and Mo) from MD02-2515, western Guaymas Basin, is investigated in conjunction with patterns in stratigraphy and productivity. High opal concentrations (~59 wt. %), representing increased diatom production, coincide with laminated sediments and dilute the concentrations of organic carbon (C_{org}) and metals. A similarity between opal and normalized C_{org}, Ag, and Cd concentrations suggests delivery to the sediments by diatom export production, while patterns in normalized Re and Mo accumulation suggest a different emplacement mechanism. Although Mo enrichment in organic-rich, laminated sediments typically represents anoxic conditions at other locations, Mo (and Re) in Guaymas Basin is enriched in nonlaminated and bioturbated sediments that are representative of oxygenated conditions. Adsorption onto Fe- and/or Mn-oxyhydroxide surfaces during oxygenation inadequately explains both the Re and Mo enrichments. Thus, recently published mechanisms invoking direct Re and Mo removal from the water column and bioturbation-assisted irrigation of Re into the sediments are used to explain the counterintuitive observations in Guaymas Basin. The MD02-2515 stratigraphic and proxy records are also different from other records in the northeast Pacific in that there is little correspondence with Greenland Dansgaard-Oeschger interstadials. There is some correlation with Heinrich events, suggesting that ventilation of intermediate waters and/or reduced productivity may be important in controlling stratigraphy and trace element accumulation. The results question whether MD02-2515 records can be compared to northeast Pacific open-margin records, especially before 17 kyr B.P.

1. Introduction

High-resolution trace element records from late Quaternary sediments have become increasingly useful for interpreting past variability in sedimentary redox conditions, primary productivity, and oxygen minimum zone (OMZ) intensity on glacial-interglacial time scales at a variety of study areas [e.g., *Ivanochko and Pedersen*, 2004; *Hendy and Pedersen*, 2005; *Dean et al*., 2006; *Cartapanis et al*., 2011]. Despite being a well-studied location, such research using trace elements within the Gulf of California (GoC) has remained scarce [e.g., *Dean et al*., 2004; *Dean*, 2006; *Cheshire and Thurow*, 2013].

The structure and composition of sediments from Guaymas Basin, in the central GoC, were first described in surface sediments and short cores (<5 kyr) [e.g., *Byrne and Emery*, 1960; *Calvert*, 1964, 1966a, 1966b]. Such early studies measured dissolved oxygen in the water column and determined that laminated sediments were only preserved where the OMZ impinged on the basin slopes. The recovery of piston cores that reached the last deglacial revealed that the sediments are not continuously laminated, illustrating that the OMZ is not a static feature [*Kelts and Nimitz*, 1982; *Keigwin and Jones*, 1990; *Pride et al*., 1999; *Keigwin*, 2002]. The top ~15–17 kyr of cores Deep Sea Drilling Project (DSDP) 480 and Giant Gravity Core (GGC) 55/Jumbo Piston Core (JPC) 56 ("JPC56") from eastern and western Guaymas Basin, respectively, are stratigraphically correlative, with alternating laminated and nonlaminated intervals. The laminated sediments are agreed to be mostly annually deposited varves [*Calvert*, 1966b; *Pike and Kemp*, 1996], while the nonlaminated intervals (also called "massive" or "homogeneous") are structureless, mottled, burrowed, or faintly laminated, suggestive of bioturbation to varying degrees [*Kelts and Nimitz*, 1982].

©2015. American Geophysical Union. All Rights Reserved.

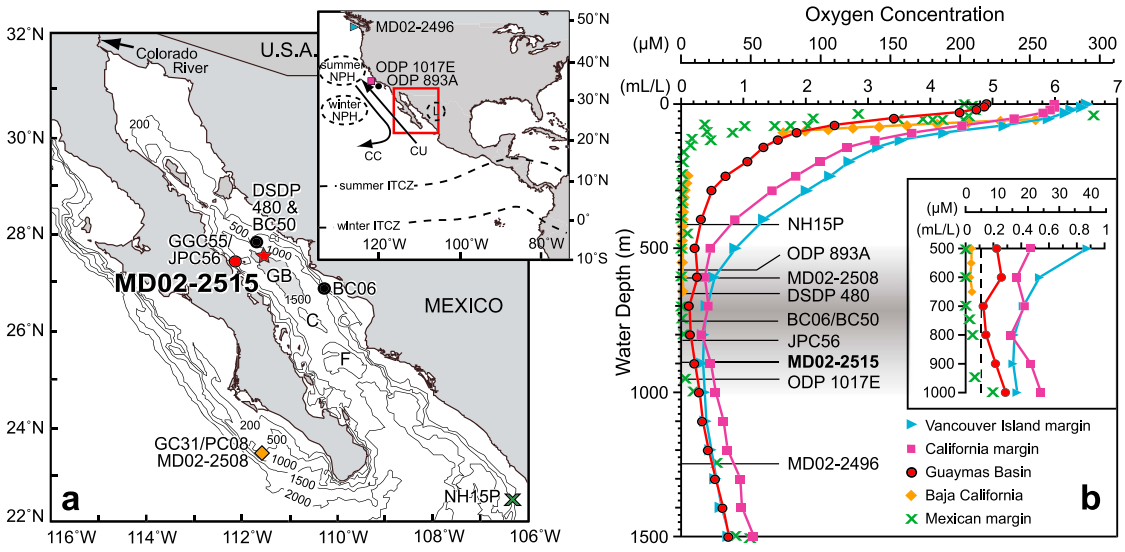

Figure 1. Coring locations discussed in this study and corresponding dissolved oxygen concentration profiles. (a) Regional map showing detail of the Gulf of California. The star indicates the location of Guaymas Basin oxygen profile in (b). Bathymetry in meters. Carmen (C) and Farallon (F) basins have depths >2000 m. The inset shows major ocean currents and seasonal atmospheric circulation. CC: California Current. CU: California Undercurrent. NPH: North Pacific High. L: North American Low (winter position). ITCZ: Intertropical Convergence Zone. (b) Coring depths and dissolved oxygen data from *Garcia et al.* [2006]. Mexican margin data from *Hartnett and Devol* [2003]. The gray zone is the approximate depth of North Pacific Intermediate Water (NPIW; 500–1000 m). The inset shows expanded oxygen profiles in the NPIW. The dashed line is 5 μM, below which laminated sediments are preserved [*Zheng et al.*, 2000].

Although microfossil and geochemical analyses from DSDP 480 and JPC56 show that the laminated sediments are compositionally different from the nonlaminated sediments [*Keigwin and Jones*, 1990; *Sancetta*, 1995; *Pride et al.*, 1999; *Barron et al.*, 2004, 2005; *Dean*, 2006], some problems arose from these observations. For example, unlike in laminated sediments elsewhere, *Dean* [2006] found in JPC56 that high biogenous silica (opal) concentrations in laminated intervals were not matched by high organic carbon (C_{org}) contents, that concentrations of Mo and Cd were not associated with the organic fraction, and that Mo and Cd enrichments did not occur in the laminated intervals. He concluded that the observed trends in Guaymas Basin sediment fabric and geochemistry were not simply controlled by productivity and sedimentary anoxia. In addition, since JPC56 covered only the last ~17 kyr, trace element deposition during the last glaciation has remained unknown.

In this study, we explore these issues and investigate recent developments in factors controlling trace element accumulation, by examining the 55 kyr long Calypso core MD02-2515, recovered from western Guaymas Basin during the 2002 International Marine Global Changes–Marges Ouest Nord Américaines (IMAGES-MONA) program [*Beaufort et al.*, 2002]. We employ a multiproxy data set including C_{org} and opal [*Pichevin et al.*, 2012], major elements [*Cheshire and Thurow*, 2013], and new high-resolution sedimentary $\delta^{15}N$ and trace Mo, Cd, Ag, and Re; the latter two metals have not been previously reported for Guaymas Basin. Comparisons are made with other high-resolution records of similar duration in the northeast Pacific Ocean, and to the Greenland ice core oxygen isotope record, in order to understand large-scale, climate-controlled changes in productivity and oxygenation.

2. Gulf of California Environmental Setting

The Gulf of California is a semienclosed, evaporitic, marginal sea connected at the southern end to the Pacific Ocean (Figure 1). Modern thermohaline circulation in the GoC involves a surface layer driven by seasonal winds, outflow of subsurface waters (50–250 m depth), and inflow of North Pacific Intermediate Water (NPIW; 500–1000 m) and Pacific Deep Water (>1000 m) [*Bray*, 1988a; *Bray and Robles*, 1991]. California Current Water (CCW), Tropical Surface Water, and Subtropical Subsurface Water (SSW) are kept at the mouth of the GoC except during the summer and El Niño events when the tropical water masses are able to penetrate further north into the GoC [*Bray*, 1988b; *Sancetta*, 1995]. The cool and fresh CCW transports subarctic waters from Vancouver Island to Baja California (Figure 1a), the oxygen-poor but nutrient-rich SSW travels north from the Eastern Tropical North Pacific (ETNP) via the California Undercurrent [*Hickey*, 1979], and the well-oxygenated

©2015. American Geophysical Union. All Rights Reserved.

NPIW is formed by cooling and sea ice formation in the subarctic North Pacific [*Talley*, 1991; *Van Scoy et al*., 1991; *Takahashi*, 1998]. SSW and NPIW are mixed with northern GoC water to produce nutrient-rich central gulf water (CGW) [*Bray et al*., 1986], which is situated over Guaymas Basin. A strong OMZ is situated at depths of 500–1000 m within the basin, with a minimum dissolved oxygen concentration of 0.13 mL/L (5.63 μM; Figure 1b) [*Garcia et al*., 2006]. The OMZ is modulated by both high productivity (>450 g C/m^2/yr) [*Kahru et al*., 2004] and the respective oxygen contents of NPIW and SSW [cf., *Wyrtki*, 1962].

The modern GoC experiences a subtropical monsoon climate defined by the seasonal positions of the Intertropical Convergence Zone (ITCZ), and the North Pacific High (NPH) and North America Low (NAL) atmospheric pressure systems (Figure 1a) [*Badán-Dangon et al*., 1991; *Thunell*, 1998]. In the winter, when these atmospheric systems are at their most southerly locations, northwesterly winds predominate over the GoC, resulting in a net outflow of surface waters [*Bray and Robles*, 1991]. Upwelling and high primary productivity occur along the eastern coastline and expand west across the GoC [*Badán-Dangon et al*., 1985], with enhanced vertical mixing and nutrient enrichment in the surface waters of the central GoC [*Delgadillo-Hinojosa et al*., 2001]. This results in deposition of opal-rich (>20%) surface sediments across the GoC, although carbonate-rich (>15%) surface sediments also occur in the western GoC [*Douglas et al*., 2007, and references therein]. In the summer, when the NPH, NAL, and ITCZ migrate northward, winds are predominantly from the south, and tropical waters enter the GoC [*Bray*, 1988b]. The water column becomes stratified, upwelling slackens, and productivity is reduced [*Thunell et al*., 1994]. Annual deposition of lithogenous material is bimodal, occurring during the summer to early autumn (July–September) and in the late winter (March) [*Thunell et al*., 1993; *Thunell*, 1998]. Eolian transport of dust from the surrounding desert is likely the main source of lithogenous material and an important source of particulate and dissolved Fe to surface waters [*Baumgartner et al*., 1991; *Segovia-Zavala et al*., 2009, 2010].

The seasonal heterogeneity in sediment supply leads to the deposition of annually laminated sediments [*Thunell et al*., 1993; *Pike and Kemp*, 1996; *Thunell*, 1998]. *Zheng et al.* [2000] found that laminated sediments on the southern California margin were preserved only when bioturbation was excluded under low bottom water oxygen conditions (<5 μM). Since minimum oxygen contents in Guaymas Basin are slightly above this threshold (Figure 1b), modern laminated sediments are likely to be partially bioturbated. El Niño events can also disrupt the seasonal pattern. Upwelling and productivity diminished, and lithogenous deposition lasted for eight months during the 1992 event [*Thunell*, 1998], while eolian Fe flux was four times higher than normal due to intense winds during the 1998 El Niño [*Segovia-Zavala et al*., 2009].

3. Methods

The 74.49 m long, 10 cm diameter MD02-2515 core was collected by the R/V *Marion Dufresne*, at 27°29.01′N and 112°04.46′W, at a water depth of 881 m (Figure 1). The age model is based on *Pichevin et al.* [2012], using 28 accelerator mass spectrometry ^{14}C measurements of bulk organic matter and two measurements made on planktonic foraminifera from undisturbed parts of the core (Figure 2). The foraminiferal ages agree well with the organic matter ages [*Pichevin et al*., 2012]. The top of the core is estimated to be at ~6.8 kyr B.P., an offset that commonly occurs for large-diameter piston corers, which typically fail to capture the uppermost sediment column. Climatic events older than ~40 kyr B.P. are interpreted with caution because of the limitations of the radiocarbon method for ages greater than seven half lives of ^{14}C and the associated large error (1σ error ± >3 kyr; Figure 2) [*McClymont et al*., 2012; *Pichevin et al*., 2012].

High-resolution geochemical analyses involved 1175 samples taken at 5 cm intervals (uncorrected core depth), which correspond to ~20–120 years per interval, depending on the sedimentation rate (Figure 2). Opal content was determined by sodium carbonate sequential leaching following *Mortlock and Froelich* [1989]. Samples for the simultaneous determination of C_{org} and total nitrogen concentrations, and $\delta^{13}C_{org}$ and $\delta^{15}N$ ratios, were decarbonated with HCl prior to analysis by continuous-flow isotope ratio mass spectrometry using a Carlo-Erba NA 2500 elemental analyzer coupled to a VG Isotech Prism mass spectrometer. Isotopic ratios are reported in the standard δ notation relative to atmospheric N_2 for nitrogen and to Pee Dee Belemnite for carbon. Instrument precision is ± 0.2‰ (1σ).

Subsamples taken at alternate 10 cm intervals, for a total of 615 samples, were used for the analyses of Ag, Cd, Re, and Mo. The isotope dilution method was used whereby 10–15 mg of dried and powdered sediment were mixed with weighed amounts of isotopically enriched and calibrated ^{109}Ag:^{107}Ag, ^{111}Cd:^{113}Cd, ^{185}Re:^{187}Re, and

©2015. American Geophysical Union. All Rights Reserved.

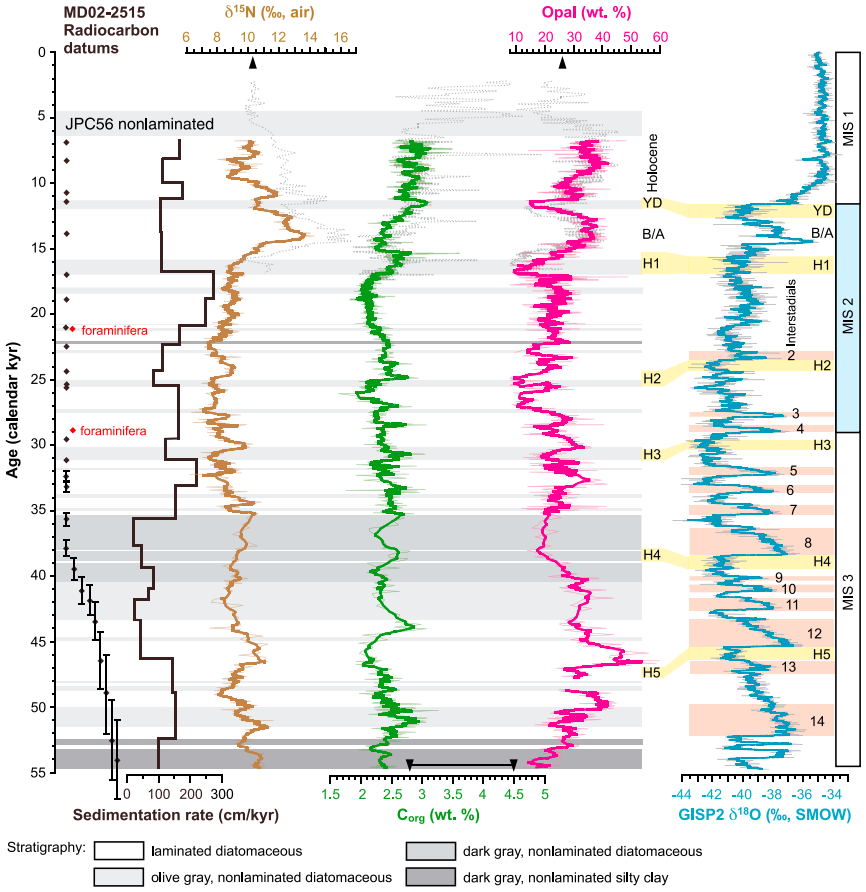

Figure 2. MD02-2515 radiocarbon datums, stratigraphy, nitrogen isotope ratios, and paleoproductivity proxies (organic carbon, C_{org}, and opal). Stratigraphy determined from *Beaufort et al.* [2002]. Radiocarbon datums (black diamonds), sedimentation rate, C_{org}, and opal data from *Pichevin et al.* [2012]. The vertical bars on datums are error ranges; datums without bars indicate error ranges spanning the height of the symbol or less. Composite GGC55/JPC56 data (dotted graph, nonlaminated layer) plotted on independently derived time scale and surface sediment values (BC06, 50, 57; black arrowheads) from *Pride et al.* [1999] and *Dean* [2006]. Climatic events identified from Greenland Ice Sheet Project (GISP) 2 record [*Stuiver and Grootes*, 2000] on the right side of the curve are the Younger Dryas (YD), Bølling/Allerød (B/A), Heinrich events (H), and Dansgaard-Oeschger interstadials (numerals) [*Dansgaard et al.*, 1993]. YD, B/A, and H events identified in MD02-2515 [*Pichevin et al.*, 2012] are plotted on the left side of the GISP2 curve. SMOW: Standard mean ocean water. Marine isotope stages (MIS) from *Lisiecki and Raymo* [2005]. The thin curves are sample data; the bold curves are five-point running averages.

^{95}Mo:^{98}Mo spike solutions (High-Purity Standards). Samples, spiked sample blanks, and a certified marine sediment standard (MESS-3; National Research Council Canada) were digested inside Teflon vials in a mixture of concentrated HCl, HNO_3, and HF acids using a Milestone Ethos EZ microwave oven, evaporated to dryness on a hotplate, and redissolved in 0.5 N HCl in the oven. Recalcitrant organic residues were dissolved with 30% H_2O_2. After a 100 µL aliquot of the final solution was extracted for Mo analyses, the remaining solutions were passed through 10 mL polypropylene anion exchange columns containing acid-conditioned Bio-rad AG 1-X8 (100–200 mesh) chloride-form resin to preconcentrate Ag, Cd, and Re and to remove polyatomic oxide interferences (^{91}Zr, ^{93}Nb, and ^{95}Mo). The final eluent was evaporated to near dryness. The Mo and Ag-Cd-Re extracts were each diluted in 1.25 mL of 1% HNO_3 and were analyzed separately with a Thermo X7 X-Series II quadrupole inductively coupled plasma mass spectrometer in peak jumping mode at the University of Victoria. Measured MESS-3 values for Ag, Cd, and Re show acceptable analytical accuracy and precision (Table 1). The measured Mo concentration is less than the certified value and is ~16% less than the average concentration reported in *Chang et al.* [2014] using the same method but with a different microwave oven. We make no attempt in this study to adjust the Mo concentrations, as Mo variability trends over time rather than the absolute Mo concentrations are compared between study sites.

©2015. American Geophysical Union. All Rights Reserved.

Table 1. Recommended and Measured Values for MESS-3 Sediment Standard

Element	Ag (ng/g)	Cd (μg/g)	Re (ng/g)	Mo (μg/g)
Recommended	180 ± 20	0.24 ± 0.01	ND[a]	2.78 ± 0.07
Measured	181 ± 11	0.21 ± 0.02	3.21 ± 0.27	2.44 ± 0.14
% Relative standard deviation	6	7.81	8.34	5.86
n	94	90	92	94

[a]ND: not determined; measured at 3.49 ± 0.31 ng/g in *Chang et al.* [2014].

Major element concentrations (Al, Fe, and Mn) were calculated from oxide concentrations determined by X-ray fluorescence spectrometry [*Cheshire and Thurow*, 2013]. A total of 131 samples were taken at ~50 cm intervals and occasionally at different sampling horizons than those analyzed for opal, C_{org}, stable isotopes, and trace elements (Table S1 in the supporting information). Correction for salt content in MD02-2515 concentrations was not applied since the highest and most variable salt content occurs in the uppermost sediment column, which the corer bypassed.

4. Results

4.1. Sediment Description

MD02-2515 consists mostly of intervals of laminated silty clay and diatomaceous silty clay that are intercalated with nonlaminated beds of various thicknesses (Figure 2). Nonlaminated intervals show evidence of bioturbation in the form of burrows and mottling; bioturbation is considered to be total where mottling is absent [*Beaufort et al.*, 2002; *Cheshire et al.*, 2005]. A multimillennial, nonlaminated interval occurs at ~35.3–43.4 kyr B.P., where the upper portion appears darker gray and is more bioturbated than the lower, lighter gray portion. There are also darker gray silty-clayey nonlaminated intervals at the bottom of the record and at ~22 kyr B.P. [*Beaufort et al.*, 2002]. Lower *b** color reflectance and higher magnetic susceptibility in the dark gray layers indicate that they are more mineral rich than lighter gray nonlaminated intervals, which in turn are more mineral rich than the laminated intervals [*Cheshire et al.*, 2005]. In the well-dated portion of the core (<40 kyr), thick (≥500 year duration) nonlaminated intervals coincide, within dating errors, with the Younger Dryas (YD) and Heinrich (H) events 1–4 (Figure 2) [*Pichevin et al.*, 2012]. Sedimentation rates range from 19 to 275 cm/kyr throughout the core, with generally higher rates in the laminated intervals (Figure 2).

4.2. Nitrogen Isotopes and Productivity Proxies

Sedimentary $\delta^{15}N$ ratios range from 6.2 to 14.3‰ throughout MD02-2515 (Figure 2). Ratios are generally depleted in the nonlaminated intervals and between 17 and 27 kyr B.P. A large increase from 10.3 to 13.4‰ at the onset of the Bølling covers a core interval of 67 cm or ~620 years of deposition. A smaller enrichment occurs at the beginning of the Holocene. In older laminated sections, $\delta^{15}N$ values never reach the maximum seen in the Bølling/Allerød (B/A).

Organic carbon contents range from 1.6 to 3.6 wt. % in MD02-2515, with higher values occurring in many but not all of the nonlaminated intervals (Figure 2). With $\delta^{13}C_{org}$ values of −21.6 to −18.3‰ (Table S1 in the supporting information), all C_{org} is assumed to be marine sourced [*Rau et al.*, 1982], indicating negligible terrigenous organic input throughout the record. Opal concentrations range from 7.5 to 59.6 wt. % throughout the core (Figure 2). Relatively high opal contents are found in many but not in all of the laminated sections, and opal is poorly correlated to C_{org} ($r = 0.14$, $p < 0.01$; Table 2a). Highest opal contents are found in the Holocene, B/A, and the section between ~45 and 50 kyr B.P. The $\delta^{15}N$, C_{org}, and opal profiles do not appear to show any visual correlation with Greenland Dansgaard-Oeschger (D-O) oscillations, especially in the older portion of the record (Figure 2). There is a good correlation between trends in MD02-2515 and JPC56 data where the two records overlap, despite different coring depths and age calibrations.

4.3. Elemental Data

All trace element concentrations in MD02-2515 are well above upper continental crust values [*McLennan*, 2001], with generally higher concentrations in the nonlaminated intervals and depleted concentrations in the laminated intervals (Figure 3). Silver concentrations range from 194 to 552 ng/g, Cd from 0.85 to 3.96 μg/g, Re from 9 to 86 ng/g, and Mo from 3 to 27 μg/g. The Ag profile is antithetical to the opal profile ($r = -0.41$, $p < 0.01$),

©2015. American Geophysical Union. All Rights Reserved.

Table 2. Pearson Correlation Coefficients (*r*) for Measured and Calculated Proxies in MD02-2515[a]

Table 2a Whole-Sediment Concentrations Where Applicable ($n = 573$)

	$\delta^{15}N$	C_{org}	Opal	Ag	Cd	Re
C_{org}	**0.32**					
Opal	**0.35**	**0.14**				
Ag	0.06	**0.18**	**−0.41**			
Cd	**0.42**	**0.29**	**0.13**	**0.34**		
Re	**0.14**	**0.29**	**−0.30**	**0.45**	**0.46**	
Mo	**0.13**	**0.18**	**−0.19**	**0.36**	**0.34**	**0.67**

Table 2b Estimated Opal-Free Concentrations Where Applicable ($n = 571$)

	$\delta^{15}N$	Opal-free C_{org}	Opal	Opal-free Ag	Opal-free Cd	Opal-free Re
Opal-free C_{org}	**0.43**					
Opal	**0.35**	**0.76**				
Opal-free Ag	**0.35**	**0.43**	**0.34**			
Opal-free Cd	**0.51**	**0.51**	**0.47**	**0.53**		
Opal-free Re	**0.21**	**0.14**	**−0.11**	**0.30**	**0.38**	
Opal-free Mo	**0.22**	**0.19**	0.07	**0.33**	**0.35**	**0.62**

Table 2c Whole-Sediment Major Element Concentrations ($n = 130$)

	Al	Fe
Fe	**0.96**	
Mn	**0.68**	**0.75**

Table 2d Estimated Opal-Free Concentrations and Metal/Al Ratios Where Applicable ($n = 121$)

	$\delta^{15}N$	Opal-free C_{org}	Opal	Opal-free Ag	Opal-free Cd	Opal-free Re	Opal-free Mo	Fe/Al
Opal-free C_{org}	**0.40**							
Opal	**0.40**	**0.70**						
Opal-free Ag	**0.29**	**0.33**	*0.22*					
Opal-free Cd	**0.46**	**0.57**	**0.43**	**0.44**				
Opal-free Re	0.17	0.09	*−0.18*	**0.27**	**0.46**			
Opal-free Mo	0.16	*0.22*	0.02	**0.28**	**0.44**	**0.55**		
Fe/Al	−0.17	−0.17	−0.10	*−0.21*	−0.10	*0.18*	**0.30**	
Mn/Al	−0.17	*−0.20*	**−0.23**	*−0.23*	−0.15	*0.22*	**0.30**	**0.48**

[a]Analyzed using SAS v. 9.4; italics: $p < 0.05$ and bold: $p < 0.01$.

and all trace elements are positively but poorly correlated with C_{org} (Table 2a). Enrichments in Re and Mo show correlations with nonlaminated intervals, regardless of mineral content, with Re showing the most distinct enrichments and depletions. Some enrichments are relatively large and abrupt, with Re increases of 20–60 ng/g from baseline levels in <200 years, and a Mo enrichment of 11 μg/g in 300 years at ~22 kyr B.P. Concentrations of Mo are similar where MD02-2515 and JPC56 records overlap; however, there is no explanation of why JPC56 Cd concentrations are 3 times higher.

The anticorrelation between Ag and opal suggests that Ag and possibly other proxies are being diluted by the high opal content, which can constitute up to half of a sample by weight. In order to highlight variability in the less abundant proxies, profiles are plotted on an opal-free basis [cf., *Calvert*, 1966a]. Large increases in whole-sediment C_{org} concentration (e.g., during YD and H1) become depleted (cf., Figures 2 and 4), and the opal-free C_{org} profile more closely resembles the opal profile ($r = 0.76$, $p < 0.01$; Table 2b), with higher opal-free C_{org} concentrations occurring in the laminated intervals. When the trace element concentrations are plotted on an opal-free basis, the shape of the Ag profile is the most transformed, Cd is somewhat affected, and the Re and Mo profiles are not changed (Figure 4). Many whole-sediment peaks in Ag and Cd concentrations in nonlaminated intervals (e.g., YD and H1 at ~36 kyr B.P.) are dampened or eliminated, and the opal-free Ag and Cd profiles show improved correlation with opal-free C_{org} ($r_{Ag} = 0.43$, $r_{Cd} = 0.51$, $p < 0.01$), opal ($r_{Ag} = 0.34$, $r_{Cd} = 0.47$, $p < 0.01$), and with each other ($r = 0.53$, $p < 0.01$; Table 2b). Estimated C_{org}/Al and metal/Al ratios produce profiles similar in shape to the opal-free profiles (Figure 4), illustrating that dilution is a

©2015. American Geophysical Union. All Rights Reserved.

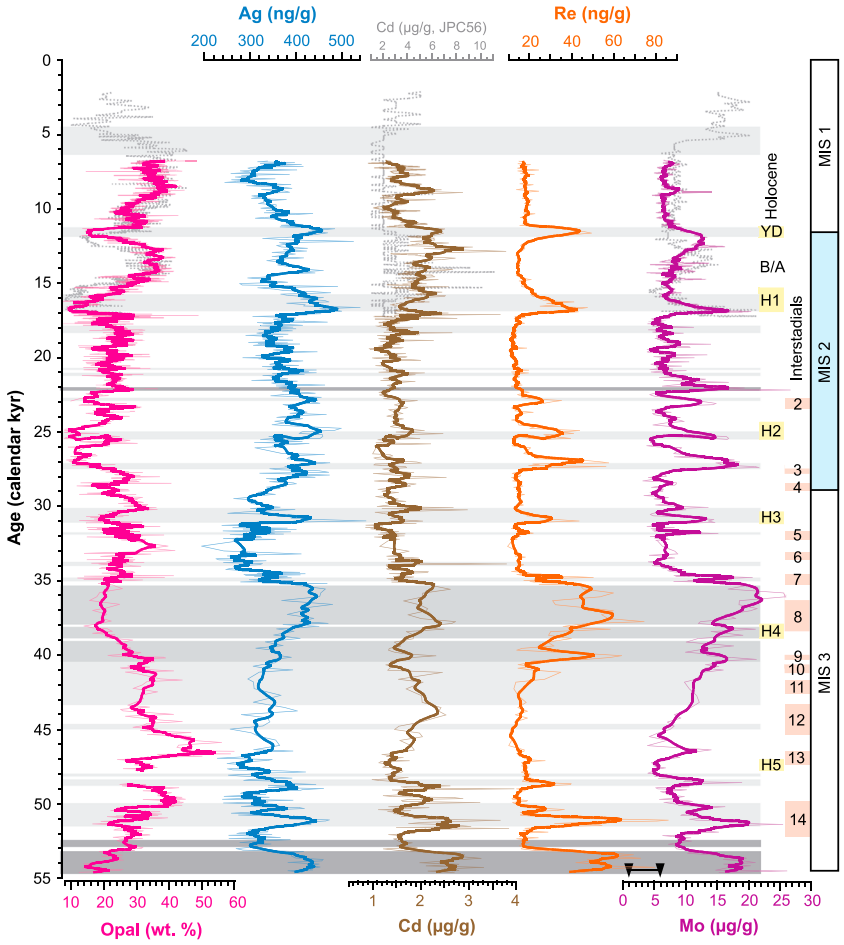

Figure 3. Whole-sediment trace element concentrations from MD02-2515 compared with opal (Figure 2). JPC56 data (dotted graph) from *Dean* [2006]; note the difference in Cd *x* axis. Surface sediment (BC06, 50) Mo concentrations (black arrowheads) from *Dean et al.* [2004]. The upper continental crust concentrations are 50 ng/g Ag, 0.098 µg/g Cd, 0.4 ng/g Re, and 1.5 µg/g Mo [*McLennan*, 2001]. See Figure 2 for the stratigraphy legend, plotting conventions, and definitions of abbreviations.

major influence, at least on C_{org}, Ag, and Cd concentrations. Neither whole-sediment nor normalized trace element concentrations show much visual resemblance with D-O oscillations (Figures 3 and 4).

Profiles of MD02-2515 Fe and Mn concentrations also do not correlate with D-O oscillations (Figure 5), but correlate well with each other ($r = 0.75$, $p < 0.01$; Table 2c), and with JPC56 profiles where there is overlap. In MD02-2515, whole-sediment Fe concentrations range from 1.4 to 3.3 wt. %, and Mn ranges from 80 to 310 ppm, all of which are below upper continental crust values of 3.5 wt. % and 600 ppm for Fe and Mn, respectively [*McLennan*, 2001]. Metal/Al profiles slightly differ from the concentration profiles. For example, distinct Fe concentration peaks during the YD and H1 are less defined in the Fe/Al profile, illustrating dilution effects due to lithogenous mineral input. That Fe/Al and Mn/Al are negatively correlated to opal and opal-free C_{org} suggests a two-phase lithogenous and biogenous contribution to the sediments (Table 2d).

5. Discussion

5.1. General Conditions of Sedimentary Trace Element Accumulation

The accumulation of chalcophile and redox-sensitive trace elements derived from biogenous and hydrogenous sources has been extensively reviewed by *Crusius et al.* [1996], *Nameroff et al.* [2002, 2004], *Tribovillard et al.* [2006], *Calvert and Pedersen* [2007], and *McKay and Pedersen* [2008]. Under oxic conditions at the sediment-water interface, trace element concentrations can remain at or below lithogenous values. As pore water oxygen becomes depleted under suboxic conditions, Re diffuses into the sediments along its concentration gradient, controlled by its removal into the solid phase due to reduction and precipitation/adsorption [*Colodner et al.*, 1993;

©2015. American Geophysical Union. All Rights Reserved.

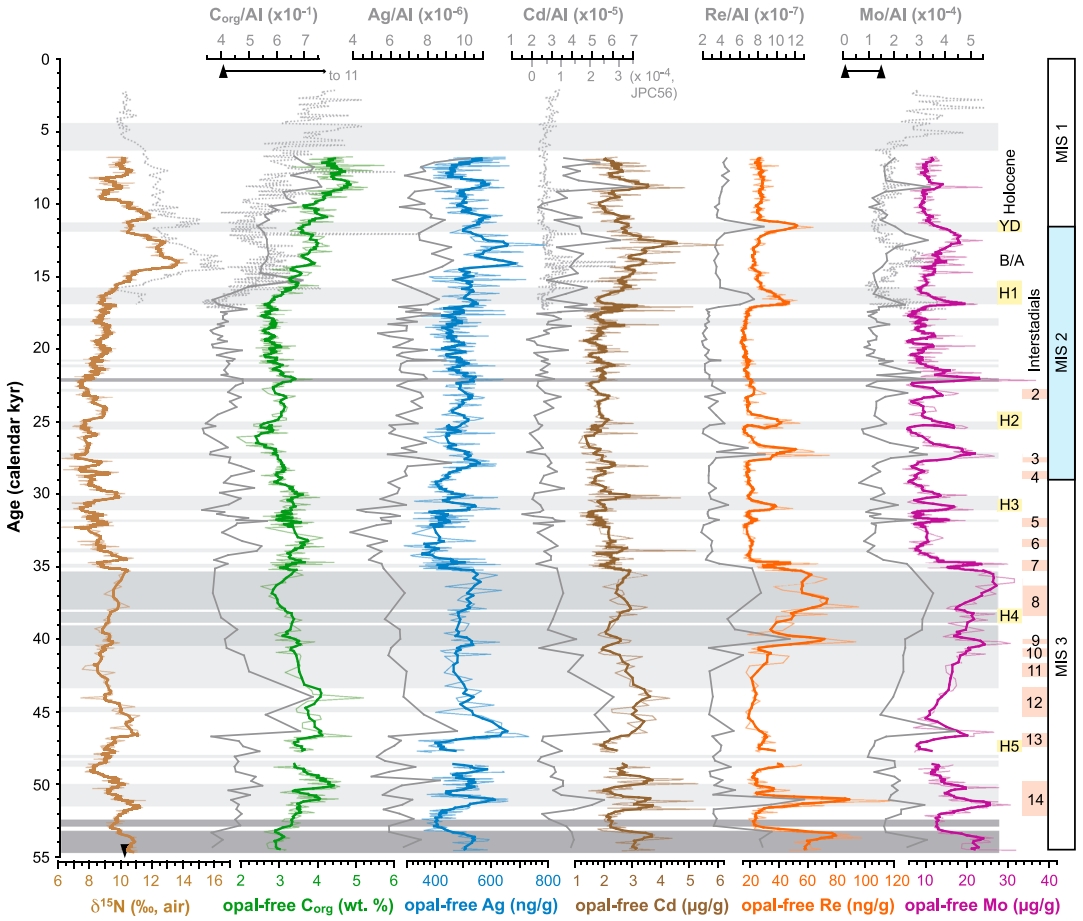

Figure 4. Estimated Al-normalized and opal-free concentrations of organic carbon (C_{org}) and trace elements from MD02-2515 compared with unaffected $\delta^{15}N$ profile (Figure 2). JPC56 data (dotted graph) from *Dean* [2006]; note the difference in Cd *x* axis. Surface sediment (BC06, 50) C_{org}/Al and Mo/Al data (black arrowheads) from *Dean et al.* [2004]. The upper continental crust metal/Al ratios are ~6×10^{-7} Ag, 1.2×10^{-6} Cd, 5×10^{-9} Re, and 1.9×10^{-5} Mo [*McLennan*, 2001]. See Figure 2 for the stratigraphy legend, plotting conventions, and definitions of abbreviations.

Crusius et al., 1996]. Of all the redox-sensitive trace elements, Re shows the largest authigenic enrichment with respect to crustal levels and is not related to Mn or Fe cycling [*Colodner et al.*, 1993; *Crusius et al.*, 1996; *Morford et al.*, 2005]. When trace amounts of pore water sulfide are present, Cd enrichment occurs when insoluble Cd sulfides precipitate [*Rosenthal et al.*, 1995; *van Geen et al.*, 1995]. Silver enrichment as highly insoluble Ag_2S [*Dyrssen and Kremling*, 1990] can occur in suboxic and anoxic sediments [*Koide et al.*, 1986; *McKay and Pedersen*, 2008]. Molybdenum can be enriched in both oxic and anoxic sediments. In oxic conditions, Mo can be adsorbed onto Fe and Mn oxyhydroxides in surface sediments [*Shimmield and Price*, 1986], resulting in simultaneous enrichments of Fe, Mn, and Mo. As oxyhydroxides dissolve during burial under suboxic conditions [*Calvert and Pedersen*, 1996], Mo can diffuse out of the sediments alongside Fe and Mn, resulting in low Mo concentrations. During anoxia, Mo immobilizes into the solid phase [*Helz et al.*, 2011] and accumulates in the sediments in the absence of Fe and Mn enrichments.

5.2. Productivity Effect on Trace Element Enrichment in Guaymas Basin

5.2.1. Diatoms and Opal Export Production

Sediment trap studies show that diatoms are the most abundant plankton group in Guaymas Basin, followed by silicoflagellates, coccolithophores, and planktonic foraminifera [*Thunell et al.*, 1996]. Dinoflagellates were not tabulated but are present in the GoC [*Price et al.*, 2013]. Because opal comprises up to 75% of the total sediment flux, and because of the clear seasonal opal signal in time series data, *Thunell* [1998] inferred that opal rather than C_{org} was more representative of productivity in Guaymas Basin. *Pichevin et al.* [2012, 2014] concluded that the discord between opal and C_{org} in Guaymas Basin arises from the preferential uptake

©2015. American Geophysical Union. All Rights Reserved.

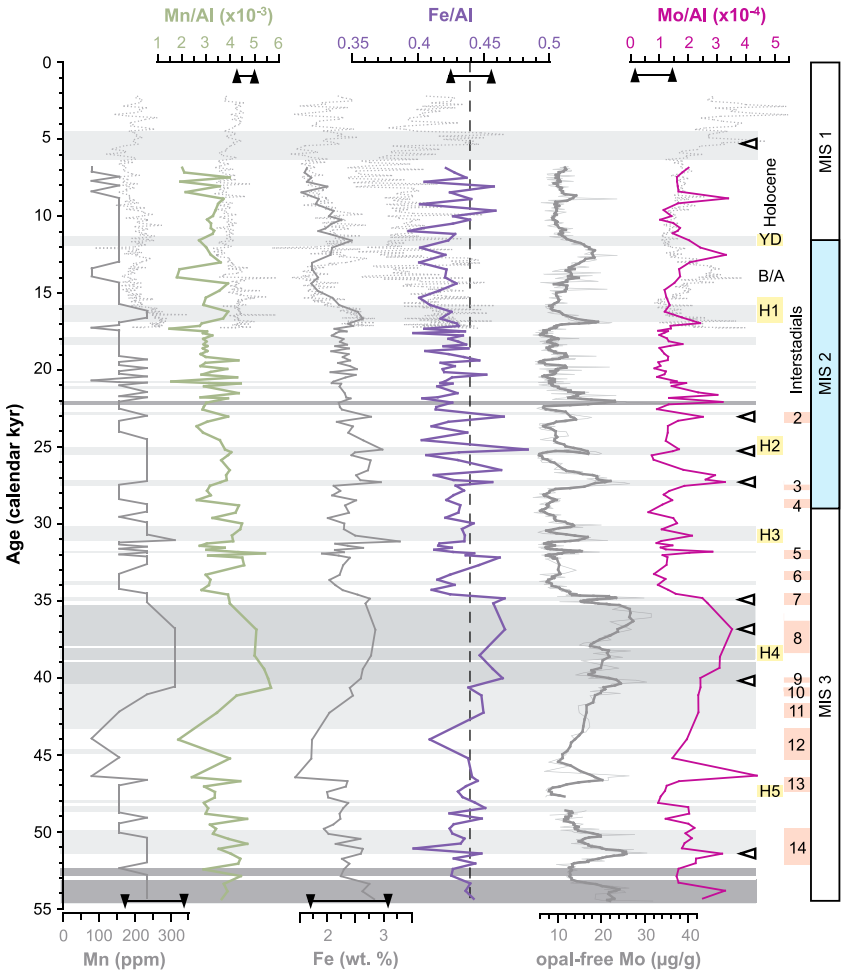

Figure 5. Major element profiles from MD02-2515 and oxyhydroxide occurrence. Original major metal oxide data from *Cheshire and Thurow* [2013]. JPC56 data (dotted graph) from *Dean* [2006]. Surface sediment (BC06, 50) metal/Al data (black arrowheads) from *Dean et al.* [2004]. The upper continental crust values are 600 ppm (7.5×10^{-3}) for Mn (Mn/Al) and 3.5 wt. % (0.44, dashed vertical line) for Fe (Fe/Al) [*McLennan*, 2001]. The white arrowheads denote possible Fe-oxyhydroxide horizons, coinciding with elevated Mo. See Figure 2 for the stratigraphy legend, plotting conventions, and definitions of abbreviations.

of Si relative to C (and N and P) by diatoms under Fe limitation during intense upwelling and blooms and results in increased export of opal relative to C_{org} to the sediments. Up to 25% of surface opal production in the GoC becomes preserved in the sediments, which is an order of magnitude greater than global ocean estimates [*Thunell et al.*, 1994]. This can explain the mismatch between opal and C_{org} concentrations described by *Dean* [2006] in JPC56 and justifies the use of opal subtraction to highlight trends in MD02-2515 C_{org}, Ag, and Cd concentration data.

Nitrogen isotope ratios are not affected by variable opal dilution (cf., Figure 4), but are influenced by processes such as relative nitrate utilization by phytoplankton in surface waters, and subsurface denitrification in the OMZs of both the GoC and ETNP [*Pride et al.*, 1999, and references therein]. Upper water column (<500 m) dissolved nitrate within Guaymas Basin is enriched (11–12‰) [*Altabet et al.*, 1999] relative to average open ocean nitrate (~5‰) [*Sigman et al.*, 1997], reflecting the import of SSW and mixing processes that produce CGW. Modern surface sediments (BC57, 27°27.21′N, 112°7.20′W, 785 m water depth) thus reflect the enriched nitrate (10.3‰) and high diatom productivity (opal ~26 wt. %) [*Pride et al.*, 1999].

5.2.2. Cadmium and Silver in Relation to Diatoms

In the northeast Pacific, the vertical profile of dissolved Cd resembles that of the algal nutrient phosphate [*Bruland et al.*, 1978]. In the central GoC, intense vertical mixing causes surface water concentrations of

©2015. American Geophysical Union. All Rights Reserved.

dissolved Cd to be two orders of magnitude higher than in northeast Pacific surface waters [*Delgadillo-Hinojosa et al*., 2001]. At depth, Cd contents in the GoC and the northeast Pacific are similar, suggesting that remineralization of organic matter within the GoC occurs mainly above 750 m [*Delgadillo-Hinojosa et al*., 2001]. In culture and field experiments, diatoms have been observed to take up Cd [e.g., *Lee et al*., 1995; *Lane and Morel*, 2000; *Cullen and Sherrell*, 2005], where it is incorporated into the cytoplasm [*Reinfelder and Fisher*, 1991].

The vertical profile of dissolved Ag in the northeast Pacific is between that of nutrient-like and scavenged elements [*Masuzawa et al*., 1989]. Silver has a strong positive correlation with silicic acid [*Zhang et al*., 2004; *Kramer et al*., 2011], but is depleted relative to silicic acid in the OMZ, which suggests Ag removal by scavenging in deeper, oxygen-poor waters [*McKay and Pedersen*, 2008]. Culture experiments show that diatoms assimilate more Ag when concentrations of nitrate, ammonium, and phosphate increase, but that only a small fraction of the Ag is incorporated into the cytoplasm [*Xu and Wang*, 2004]. This suggests that a larger fraction of Ag is incorporated into the frustule, but there are no direct observations to confirm this. Nevertheless, the strong correlation between Ag and silicic acid has prompted the proposal that diatoms are the likely vectors for Ag delivery to the sediments [e.g., *Hendy and Pedersen*, 2005; *Wagner et al*., 2013]. No water column dissolved Ag data are available from the GoC.

5.2.3. Productivity Indicators in MD02-2515

High opal concentrations and enriched δ^{15}N in MD02-2515 likely represent increased diatom productivity and better opal export and preservation, e.g., during the laminated Holocene, B/A, and the interval between 45 and 50 kyr B.P. (Figure 2). Conversely, lower opal concentrations and depleted δ^{15}N likely reflect reduced diatom productivity, such as during marine isotope stage (MIS) 2 or in nonlaminated sediments. These assumptions are supported by diatom records from JPC56 and DSDP 480, which showed lower abundance of typical winter-bloom species and higher occurrences of advected tropical species in nonlaminated intervals of the YD and H1 and reversed trends in laminated sediments of the B/A and Holocene [*Sancetta*, 1995; *Barron et al*., 2004, 2005]. New diatom data from MD02-2515 show reduced biosiliceous productivity during older H events and reduced abundance of winter-upwelling species throughout MIS 2 [*Barron et al*., 2014]. Thus, changes in total diatom production should similarly affect the accumulation of opal, C_{org}, Ag, and Cd in the sediments. Yet the correlation of opal-free Ag and Cd with opal is only moderate (Table 2b), suggesting that other factors, such as variable diatom nitrate uptake [*Pride et al*., 1999; *Xu and Wang*, 2004], remineralization of organic detritus in the water column [*Delgadillo-Hinojosa et al*., 2001], scavenging by sinking organic particles [*McKay and Pedersen*, 2008], or the amount of sulfide in the sediments [*Koide et al*., 1986; *van Geen et al*., 1995], also affected Ag and Cd delivery and accumulation.

5.3. The Molybdenum Conundrum and the Rhenium Problem in Guaymas Basin

In contrast to Ag and Cd, the behaviors of dissolved Re and Mo are conservative in the water column [*Collier*, 1985; *Anbar et al*., 1992; *Singh et al*., 2011], because Re has no known biological use, and biological Mo usage is likely small compared to the available Mo supply [*Nameroff et al*., 2002]. These factors may be why the whole-sediment and opal-corrected Re and Mo profiles in the MD02-2515 record are similar (Figures 3 and 4).

5.3.1. Contradictions Between Mo and Re Enrichments and Guaymas Stratigraphy

Enriched authigenic Mo in sediments has been identified elsewhere as the diagnostic proxy for past anoxic conditions, especially when associated with organic-rich and laminated sediments [e.g., *Zheng et al*., 2000; *Algeo and Lyons*, 2006; *Dean et al*., 2006]. Rhenium is a proxy for suboxic conditions because it experiences reduction at less negative potentials and shallower sediment depths than Mo [*Crusius et al*., 1996, 1999; *Morford et al*., 2005]. Thus, higher Mo and Re concentrations in older Guaymas Basin nonlaminated sediments are counterintuitive because nonlaminated intervals represent oxygenated conditions, as indicated by bioturbation. Recent sediments also show this contradiction. Laminated box cores BC06 and BC50 (~30–40 cm length; Figure 1a) dated from the early A.D. 1880s to 1990s [*Thunell et al*., 1994] have sedimentary Mo concentrations of 3 ± 2 ppm (n = 87, BC06) and 9 ± 3 ppm (n = 65, BC50) [*Dean et al*., 2004], which are similar to whole-sediment baseline Mo concentrations in MD02-2515 laminated intervals (Figure 3). Likewise, box cores recovered at 415–800 m water depth near DSDP 480 contain higher pore water Mo levels in laminated sediments (124 ± 11 ppb, core E-9; 69 ± 33 ppb, core E-13; each n = 3) than in bioturbated sediments (58 ± 12 ppb, n = 3, core E-5) at 10–20 cm below the sediment-water interface [*Brumsack and Gieskes*, 1983], indicating that less Mo is being fixed into the laminated sediments.

©2015. American Geophysical Union. All Rights Reserved.

Table 3. Modeled Precipitation Depths and Re and Mo Concentrations (*J*/MAR) in Sediments, as Compared to Observed Concentrations in MD02-2515 and Recent Sediments

Sediment structure[a]			Laminated				Nonlaminated				Laminated
Time interval[a]			mid-Holocene		below H1		YD		MIS 3		A.D. 1810–1990[g]
Sedimentation rate (cm/kyr)[a]			166		275		107		19		180[g]
Estimated MAR (g/cm^2/kyr)[b]			44		73		28		5		38[g]
z (cm)[c]	Re *J*[d]	Mo *J*[d]	Re (ng/g)[e]	Mo (μg/g)[e]	Re (ng/g)	Mo (μg/g)	Re (ng/g)	Mo (μg/g)	Re (ng/g)	Mo (μg/g)	Mo (μg/g)
0.5	2000	3006	46	69	28*	41	71	107	396	596	80
0.75	1333	2004	30*[f]	46	18*	28	47*	71	264	397	53
1	1000	1503	23**[f]	34	14**	21	36**	53	198	298	40
1.5	667	1002	15**	23	9	14*	24	36	132	199	27
2	500	752	11	17*	7	10*	18	27*	99*	149	20**[g]
5	200	301	5	7**	3	4**	7	11**	40**	60	8**[g]
7.5	133	200	3	5**	2	3	5	7	26	40*	5**[g]
10	100	150	2	3	1	2	4	5	20	30**	4**[g]

[a]Refer to Figure 2 for the stratigraphy, time intervals, and sedimentation rates (see also Table S1 in the supporting information).
[b]Estimated MAR (mass accumulation rate) = DBD * sedimentation rate, where
DBD (dry bulk density) = (1–Φ) * grain density = 0.26 g/cm^3;
Φ (porosity) = 0.9 [*Ivanochko and Pedersen*, 2004]; and
grain density = 2.64 g/cm^3 (average for MD02-2515) [*Beaufort et al.*, 2002].
[c]*z* = depth in sediments from sediment-water interface, where Re and Mo precipitate and pore water Re and Mo reduce to zero.
[d]$J = (\Phi/F)D_b(\partial C/\partial z)$ (Fick's first law for downward diffusion) = diffusion flux (Re: ng/cm^2/kyr, Mo: μg/cm^2/kyr), where
Φ (porosity) as defined above;
F (formation factor) = 1.3 [*Manheim*, 1970];
D_b (diffusion coefficient) = 6×10^{-6} cm^2/s (Re) and 7×10^{-6} cm^2/s (Mo) [*Li and Gregory*, 1974];
C (dissolved concentration) = 40 pmol/kg (Re) [*Anbar et al.*, 1992] and 100 nmol/kg (Mo) [*Sohrin et al.*, 1987]; and
z (sediment depth) as defined above.
[e]*J*/MAR ratio is the concentration of Re (ng/g) or Mo (μg/g) enriched in the sediments at the indicated *z*.
[f]Whole-sediment (**) and opal-free (*) concentrations similar to observed values in MD02-2515 (Figures 3 and 4), accumulating at indicated *z*.
[g]Box core BC50 data from *Thunell et al.* [1994], Mo compared to data from *Dean et al.* [2004], and Re not determined.

The flux of Mo and Re into laminated versus nonlaminated sediments in Guaymas Basin can be estimated using Fick's first law for downward diffusion, and the concentrations of Re and Mo accumulating in the sediments can be determined as the quotient of the flux and the sediment mass accumulation rate (MAR; Table 3). The MAR is dependent on sedimentation rate, which is higher in laminated intervals (Figure 2). All other parameters remaining constant, the calculated enrichment of Re to concentrations observed in the MD02-2515 record always occurs at shallower sediment depths (mostly 0.5–1 cm) than observed Mo enrichment (mostly 2–5 cm depth), as expected, regardless if whole-sediment or opal-free concentrations are considered and regardless of sedimentation rates (Table 3 and cf., Figures 3 and 4). However, the higher sedimentation rates in both recent and older laminated intervals do lead to lower Re and Mo concentrations, confirming the unusual observations in Guaymas Basin.

A logical conclusion for the greater Mo enrichments in the bioturbated and nonlaminated sediments is that Mo is associated with the deposition of Fe or Mn oxyhydroxides during oxygenated conditions [cf., *Shimmield and Price*, 1986]. However, Mn/Al ratios throughout MD02-2515 fall below upper continental crust levels, not all Fe/Al increases are associated with Mo enrichments, and many Mo increases are accompanied by depleted Fe/Al ratios (Figure 5). Only when Fe and Mo are simultaneously elevated is it possible that oxygenated conditions resulted in Mo adsorption onto Fe-oxyhydroxide surfaces. Still, this explanation is insufficient for explaining Re enrichment in nonlaminated intervals.

5.3.2. Recent Modeling of Mo and Re Precipitation

Helz et al. [2011] suggest that dissolved Mo is removed from sulfidic waters as a previously undetected, nanoscale Fe(II)–Mo(VI) sulfide (Fe-Mo-S) solid phase. Assuming sufficient reactive Fe supply and a constant ionic strength, the model predicts that in an acidic water column (pH < 7), as occurs during biological sulfate reduction, Mo can be efficiently precipitated from seawater over a wide H_2S concentration range (10^{-5} to 10^{-3} M), as long as H_2S levels are not too high to counteract efficiency (e.g., $>10^{-3}$ M; Figure 8 in *Helz et al.* [2011]). In alkaline lakes (pH > 8.5), dissolved Mo can be evaporatively concentrated to values much greater

©2015. American Geophysical Union. All Rights Reserved.

than in average seawater (~100 nmol/kg) [*Sohrin et al*., 1987], also facilitating Mo removal from the aqueous phase. *Helz and Dolor* [2012] suggest that Re is not simply reduced under suboxic conditions. Based on similarities between Re and Mo behavior in the Black Sea, Re is suggested to coprecipitate in the water column with the nanoscale Fe-Mo-S phase in the presence of sulfide. Because this phase is too small to settle directly to the sediments, it must be scavenged by sinking organic matter. *Morford et al.* [2012] showed that irrigation of near-surface, coastal sediments by bioturbation can augment the diffusive flux of Re across the sediment-water interface by transporting dissolved Re in bottom waters into Re-deficient anoxic pore waters. Exposure of the sediments to oxygenated bottom waters via irrigation yielded no net remobilization of authigenic Re on seasonal time scales [*Morford et al*., 2009]. Accumulation of Re occurred as long as there was a sufficient C_{org} oxidation rate and a shallow ($<$1 cm) oxygen penetration depth [*Morford et al*., 2005, 2009, 2012].

Thus, in an evaporitic and productive basin like Guaymas Basin, it is possible that there is a combination of both enhanced Re and Mo coprecipitation and diffusive flux into the sediments. For example, when nonlaminated sediments were deposited during reduced productivity and/or better ventilation, water column pH and dissolved H_2S concentrations could have become optimized to promote efficient removal of Mo and Re from the water column [*Helz et al*., 2011]. Increased eolian Fe input [e.g., *Segovia-Zavala et al*., 2009] and/or reduced uptake of Fe by diatoms [*Pichevin et al*., 2012] could have supplied more reactive Fe to promote further Fe-Mo-S and Re coprecipitation, while lower sedimentation rates, along with irrigation by bioturbation, decreased the path of diffusion of Re and Mo into the sediments. The sediments must have remained sufficiently reducing for Re and Mo to remain in solid phase, even during better ventilated water column conditions, such as those inferred during H events in Guaymas Basin. Further geochemical measurements in the water column and at the sediment-water interface are required to constrain the relative importance of processes governing Re and Mo precipitation and accumulation in Guaymas Basin.

5.4. Late Quaternary Guaymas Environment History and NE Pacific Context

5.4.1. Holocene and Deglacial (~2 to 17 kyr B.P.)

Given the lack of opal data at some sites, C_{org} is used to compare productivity. C_{org} profiles among northeast Pacific sites, except in Santa Barbara Basin, are mostly similar, with higher concentrations in the B/A and Holocene, and lower concentrations in the YD and H1, regardless of the presence of laminations (Figure 6). The similarities of the C_{org} records with the upper 17 kyr of the Greenland Ice Sheet Project (GISP) 2 record suggest a teleconnection between North Atlantic and Pacific ocean-climate conditions and a common control on productivity (section 5.4.3). The Mo profile in Guaymas Basin, however, differs from all other sites, reflecting the unique redox conditions for Mo accumulation in Guaymas Basin.

In the GoC, abundant winter-bloom diatom species and high opal in laminated sediments of the B/A and early Holocene suggest that productivity and upwelling were more intense than today, with northwesterly winter winds and strong upwelling persisting into the spring [*Sancetta*, 1995; *Barron et al*., 2005], as confirmed by sea surface temperature (SST) proxies $U_{37}^{K'}$ and TEX_{86}^{H} from MD02-2515 that show a cooler and mixed water column [*McClymont et al*., 2012]. Enriched $\delta^{15}N$ values suggest less ocean ventilation and/or increased denitrification in the ETNP and within the GoC [cf., *Pride et al*., 1999]. In contrast, lower opal and increased tropical diatom and dinoflagellate species in nonlaminated sediments of the YD and H1 [*Sancetta*, 1995; *Barron et al*., 2005; *Price et al*., 2013] suggest a more El Niño-like climate, with warm and nutrient-poor tropical waters present year-round [*Pride et al*., 1999]. SST proxies show that water-column stratification and warming occurred at the onset of both bioturbated intervals, contradicting cooling observed elsewhere in the northeast Pacific, and suggesting that temperature trends in Guaymas Basin are more similar to southern hemisphere warming [*McClymont et al*., 2012].

5.4.2. The Last Glacial Maximum (~17–29 kyr B.P.)

The Guaymas Basin record shows some of the lowest C_{org} concentrations during the Last Glacial Maximum (LGM), similar to what is observed on the open margin (Figure 6). The low concentrations and depleted $\delta^{15}N$ values suggest that productivity was reduced at all sites during the LGM [cf., *Ganeshram and Pedersen*, 1998; *Hendy et al*., 2004; *Chang et al*., 2008; *Cartapanis et al*., 2011] and that there was reduced denitrification and/or less export of enriched nitrate from the ETNP [*Pride et al*., 1999; *Hendy et al*., 2004]. Modeling suggests that the continental ice sheet and cool air temperatures could have led to the establishment of an anticyclonic cell over North America [*Romanova et al*., 2006], the weakening of the NPH [*Ganeshram and Pedersen*, 1998], or the failure of NPH migration or the southward displacement of the ITCZ [*Cheshire and Thurow*, 2013]. These

©2015. American Geophysical Union. All Rights Reserved.

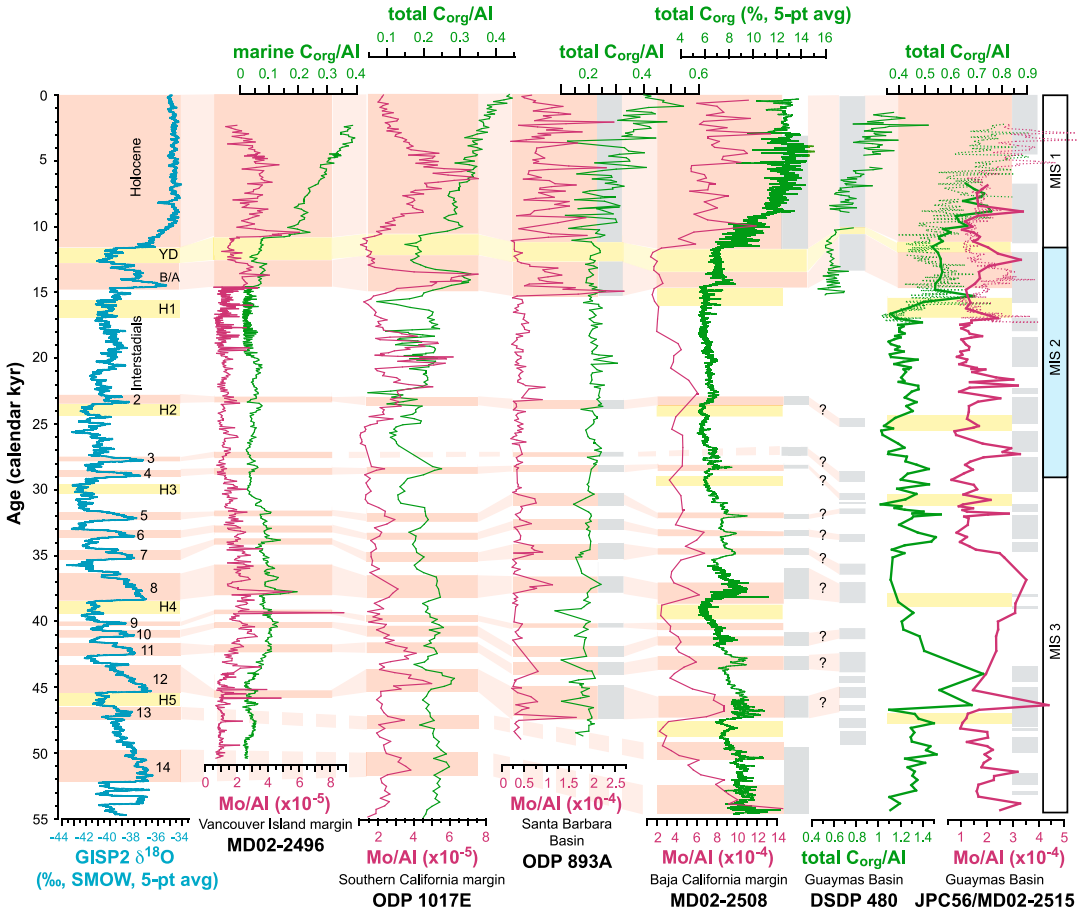

Figure 6. Comparison of climate, stratigraphy, C_{org}, and Mo from coring sites in the northeast Pacific (Figure 1); low-resolution NH15P data are not shown [cf., *Ganeshram and Pedersen*, 1998]. The red horizontal bands are warm climate intervals, and the yellow horizontal bands are cool climate intervals identified from GISP2. The dashed banding and question marks denote climate correlations not identified in the original studies. The gray bands are intervals of laminated sediments; the white areas or no banding denote nonlaminated sediments. Note the inverted shading of laminated intervals in MD02-2515 (cf., Figures 2–5). Data from MD02-2496 [*Chang et al.*, 2008, 2014], ODP 1017E [*Hendy et al.*, 2004; *Hendy and Pedersen*, 2005], ODP 893A [*Behl and Kennett*, 1996; *Ivanochko and Pedersen*, 2004], MD02-2508 [*Cartapanis et al.*, 2011], DSDP 480 [*Barron et al.*, 2004], and JPC56 (dotted graph) [*Dean*, 2006] are plotted on independently calibrated time scales. DSDP 480 stratigraphy redrawn from *van Geen et al.* [2003].

scenarios likely resulted in a weakened California Current along the coast [*Doose et al.*, 1997; *Herbert et al.*, 2001] and weakened upwelling winds and productivity within the GoC [*Cheshire and Thurow*, 2013]. Baseline Mo concentrations in MD02-2515, however, remain similar between glaciation and the early to mid-Holocene, despite the changing C_{org} concentrations, which again is contradictory to what is observed at other sites (Figure 6).

Glacial-stage stratigraphy in MD02-2515 also differs from open-margin sites, including the nearby Mexican (core NH15P; Figure 1) [*Ganeshram and Pedersen*, 1998; *Nameroff et al.*, 2002] and Baja California margins (cores GC31/PC08 and MD02-2508; Figure 1) [*Dean et al.*, 2006; *Cartapanis et al.*, 2011], which are all predominantly nonlaminated during the LGM (Figure 6). Based on evidence that supports a deeper ventilation depth for the NPIW during the last glacial (1000–4000 m) [*Keigwin*, 1998; *Herguera et al.*, 2010], and a stagnant water column at depths of the modern NPIW (500–1000 m), *Cartapanis et al.* [2011] explain the lack of laminations on the Baja California margin as a result of decreased productivity (i.e., reduced sediment heterogeneity), despite a more intense OMZ than today [*Dean et al.*, 2006]. Decreased productivity may also explain the lack of LGM laminations at DSDP 480, but not at MD02-2515, where productivity persisted throughout the LGM, as indicated by glacial opal concentrations that are not greatly reduced from today's levels (Figure 2). This suggests different upwelling, productivity, and oxygenation regimes between eastern and western Guaymas Basin over time [cf., *Douglas et al.*, 2007]. Such east-west divergences in geochemistry and microfossil assemblages occurred in Guaymas Basin after 6.2 kyr B.P. as a result of a shift toward modern

©2015. American Geophysical Union. All Rights Reserved.

conditions where wind patterns favored late winter-early spring upwelling and biosiliceous productivity on the eastern side of Guaymas Basin [*Barron et al*., 2005]. Thus, biosiliceous productivity was likely favored on the western side during the LGM.

5.4.3. Marine Isotope Stage 3 and D-O Oscillations

The most obvious features during MIS 3 are the D-O oscillations, which are seen elsewhere in the northeast Pacific, regardless if the sediments are laminated or not, but are not seen in MD02-2515 (Figures 2–6). The overprinting of millennial-scale North Atlantic climate events onto northeast Pacific sediment records has been explained by a variety of teleconnections, including changes in atmospheric [e.g., *Hostetler et al*., 1999] or thermohaline circulation [e.g., *Alley and Clark*, 1999], or freshening of the North Atlantic affecting deep-sea nutrients, primary productivity, and the OMZ [e.g., *Schmittner et al*., 2007]. Heinrich event signatures seen in North Pacific records were explained by the propagation of increased westerly winds over Eurasia to the North Pacific [*Clement and Peterson*, 2008].

Similarities between open-margin records in the northeast Pacific have also been explained by the connecting influence of the California Undercurrent [*Kienast et al*., 2002; *Chang et al*., 2008; *Galbraith et al*., 2008], which flows poleward year-round and transports oxygen-poor SSW from the ETNP to as far north as the Aleutian Islands [*Thomson and Krassovski*, 2010]. Coastal upwelling draws nutrients from the depth of the SSW, and increased nutrient levels and/or Undercurrent strength during warm interstadials resulted in synchronous enrichments in $\delta^{15}N$, C_{org}, and Mo, and occasionally the presence of laminations (Figure 6) [cf., *Chang et al*., 2008, 2014].

Warmer climates would have also diminished NPIW formation, through warmer SST and the reduction of sea ice and brine formation, resulting in a more oxygen-depleted water column at intermediate depths (500–1000 m) [cf., *Cartapanis et al*., 2011]. While the Ocean Drilling Program (ODP) 893A record shows remarkable fidelity between laminated intervals and Greenland interstadials [*Behl and Kennett*, 1996], ODP 893A is anomalous in that increases in C_{org} concentrations do not always coincide with elevated Mo concentrations (Figure 6). This has been explained by regional changes in the NPIW having a greater effect on sedimentary anoxia than does local productivity and the semienclosed nature of the Santa Barbara Basin limiting the flow of local currents [*Ivanochko and Pedersen*, 2004].

Why MD02-2515 stratigraphy and geochemical records differ from those on the open margin can be similarly explained. Like Santa Barbara Basin, the GoC is also restrictive to currents. Perhaps the depth at which MD02-2515 was recovered is also more sensitive to changes in NPIW than to SSW, the latter missing the upwelling season in the GoC by entering only during the less productive summer months and El Niño events [*Sancetta*, 1995]. This may be why MD02-2515 opal, C_{org}, Ag, and Cd (productivity) do not record D-O oscillations. Increased ventilation of NPIW during H events [cf., *Chikamoto et al*., 2012] may explain why MD02-2515 Re and Mo (redox conditions) correlate better, but not perfectly, with nonlaminated sediments deposited during H events. However, Re and Mo enrichments in nonlaminated intervals not associated with H events (e.g., ~35–40 kyr B.P.) may also reflect sensitivity of the western GoC to localized ventilation events and/or reduced productivity (lower opal) associated with El Niño-like conditions. A geochemical assay of the full DSDP 480 record would provide a useful comparison for the eastern side.

6. Summary and Conclusion

High-resolution sediment stratigraphy, nitrogen isotopes, and opal, organic carbon (C_{org}), and major and trace element accumulation patterns from core MD02-2515 suggest unique productivity and redox conditions within western Guaymas Basin that are not seen on the open northeast Pacific margin. The high opal content of Guaymas Basin sediments (up to 59 wt. %) dilutes all other concentration parameters. Normalization eliminates the opal-C_{org} mismatch and somewhat explains the incongruity between Cd, C_{org}, and laminated intervals both observed by *Dean* [2006] but does not explain Mo and Re enrichments in nonlaminated sediments. While opal and normalized C_{org}, Ag, and Cd patterns throughout MD02-2515 suggest an association with diatom export productivity, normalized Re and Mo patterns appear to respond to changes in bottom water dissolved oxygen concentrations as a function of changes in productivity and/or ventilation. The relative enrichments of Re and Mo in Guaymas Basin nonlaminated sediments are an unusual reversal not seen in laminated sediment records elsewhere and invoke a complex process of Re and Mo emplacements within Guaymas Basin that may involve a combination of direct removal from seawater into solid phase [*Helz et al*., 2011;

©2015. American Geophysical Union. All Rights Reserved.

Helz and Dolor, 2012] and enhanced diffusion flux across the sediment-water interface via reduced sedimentation rates and irrigation by bioturbation [*Morford et al.*, 2012], during times of increased ocean ventilation (e.g., H events) and/or reduced productivity during El-Niño-like conditions. The adsorption of Mo onto oxyhydroxide surfaces during such oxygenated conditions is remote, due to the low occurrence of coincident increases in Mo, Fe, and Mn.

The incongruity between the MD02-2515 records with eastern Guaymas Basin stratigraphy (DSDP 480), and with records on the open northeast Pacific margin before ~17 kyr B.P., suggests that productivity and redox conditions operated differently between western and eastern Guaymas Basin and independently from the open margin during the glacial stage. *van Geen et al.* [2003] recognized the difficulty of relating laminations and oxygenation histories from a silled basin (e.g., Santa Barbara Basin) to open-ocean conditions. While these authors had classified Guaymas Basin cores DSDP 480 and JPC56 with the "open-margin" set, our findings suggest that western Guaymas Basin is unlike the open margin and should be classified separately, meaning that the productivity and redox history from MD02-2515 should be cautiously compared to the open margin, especially before ~17 kyr B.P.

Acknowledgments

We thank the crew and shipboard scientific party of the R/V *Marion Dufresne* (MD126 MONA IMAGES VIII) for recovering and handling core material. R. Dwyer subsampled MD02-2515 for trace element analysis. A. Krepakevich and J. Spence performed trace element preparation and analysis, respectively. W. Dean, E. McClymont, V. Pospelova, A. Price, and R. Thunell provided helpful discussions; J. Barron, O. Cartapanis, H. Cheshire, W. Dean, H. Hartnett, I. Hendy, and T. Ivanochko shared data. Special thanks go to S. Calvert for enlightening discussions and for reviewing earlier drafts of the manuscript. Two anonymous reviewers provided constructive criticism. Funding for this project was provided by the Natural Sciences and Engineering Research Council of Canada and the Canadian Foundation for Climate and Atmospheric Sciences (CFCAS) to T.F.P. and the Natural Environmental Research Council to R.G. This work is a contribution to the Polar Climate Stability Network of CFCAS. Supporting information are available from Panagea (http//:www.pangaea.de). This manuscript was dedicated to S. Calvert on the occasion of the 50th anniversary of his seminal work in the Gulf of California [Calvert, 1964].

References

Algeo, T. J., and T. W. Lyons (2006), Mo total organic carbon covariation in modern anoxic marine environments: Implications for analysis of paleoredox and paleohydrogeographic conditions, *Paleoceanography*, *21*, PA1016, doi:10.1029/2004PA001112.

Alley, R. B., and P. U. Clark (1999), The deglaciation of the northern hemisphere, *Annu. Rev. Earth Planet. Sci.*, *27*, 149–182, doi:10.1146/annurev.earth.27.1.149.

Altabet, M. A., C. Pilskaln, R. Thunell, C. Pride, D. Sigman, F. Chavez, and R. François (1999), The nitrogen isotope biogeochemistry of sinking particles from the margin of the eastern North Pacific, *Deep Sea Res., Part I*, *46*, 655–679, doi:10.1016/S0967-0637(98)00084-3.

Anbar, A. D., R. A. Creaser, D. A. Papanastassiou, and G. J. Wasserburg (1992), Rhenium in seawater: Confirmation of generally conservative behavior, *Geochim. Cosmochim. Acta*, *56*, 4099–4103, doi:10.1016/0016-7037(92)90021-A.

Badán-Dangon, A., D. J. Koblinsky, and T. Baumgartner (1985), Spring and summer in the Gulf of California: Observations of surface thermal patterns, *Oceanol. Acta*, *8*, 13–22.

Badán-Dangon, A., C. E. Dorman, M. A. Merrifield, and C. D. Wianat (1991), The lower atmosphere over the Gulf of California, *J. Geophys. Res.*, *96*, 16,877–16,896, doi:10.1029/91JC01433.

Barron, J. A., D. Bukry, and J. L. Bischoff (2004), High resolution paleoceanography of the Guaymas Basin, Gulf of California, during the past 15,000 years, *Mar. Micropaleontol.*, *50*, 185–207, doi:10.1016/S0377-8398(03)00071-9.

Barron, J. A., D. Bukry, and W. E. Dean (2005), Palaeoceanographic history of the Guaymas Basin, Gulf of California, during the past 15,000 years based on diatoms, silicoflagellates, and biogenic sediments, *Mar. Micropaleontol.*, *56*, 81–102, doi:10.1016/j.marmicro.2005.04.001.

Barron, J. A., D. Bukry, and H. Cheshire (2014), Response of diatom and silicoflagellate assemblages in the central Gulf of California to regional climate change during the past 55 kyr, *Mar. Micropaleontol.*, *108*, 28–40, doi:10.1016/j.marmicro.2014.02.004.

Baumgartner, T. R., V. Ferreira-Bartrina, and P. Moreno-Hentz (1991), Varve formation in the central Gulf of California: A reconsideration of the origin of dark laminae from the 20th century varve record, in *The Gulf and Peninsular Province of the Californias*, *Mem.*, vol. 47, edited by J. P. Dauphin and B. R. T. Simoneit, pp. 617–635, Am. Assoc. of Pet. Geol., Tulsa, Okla.

Beaufort, L., et al. (2002), Les rapports des campagnes à la mer, MD 126 MONA IMAGES VIII Cruise Report, Institute Polaire Fr. Paul-Emile Victor, Plouzaneé, France. [Available at http://www.images-pages.org/cruises/images8/MONA_Cruise_Report.pdf.]

Behl, R. J., and J. P. Kennett (1996), Brief interstadial events in the Santa Barbara basin, NE Pacific, during the past 60 kyr, *Nature*, *379*, 243–246, doi:10.1038/379243a0.

Bray, N. A. (1988a), Thermohaline circulation in the Gulf of California, *J. Geophys. Res.*, *93*, 4993–5020, doi:10.1029/JC093iC05p04993.

Bray, N. A. (1988b), Water mass formation in the Gulf of California, *J. Geophys. Res.*, *93*, 9223–9240, doi:10.1029/JC093iC08p09223.

Bray, N. A., and J. M. Robles (1991), Physical oceanography of the Gulf of California, in *The Gulf and Peninsular Province of the Californias*, *Mem.*, vol. 47, edited by J. P. Dauphin and B. R. T. Simoneit, pp. 511–553, Am. Assoc. of Pet. Geol., Tulsa, Okla.

Bray, N. A., M. C. Hendershott, J. M. Robles, and A. C. Carrasco (1986), *Pichicuco 6: Gulf of California CTD Data Report, R/V New Horizon*, November 1984, 260 pp., Scripps Institute of Oceanography, La Jolla, Calif.

Bruland, K. W., G. A. Knauer, and J. H. Martin (1978), Cadmium in the northeast Pacific waters, *Limnol. Oceanogr.*, *23*, 618–625.

Brumsack, H. J., and J. M. Gieskes (1983), Interstitial water trace-metal chemistry of laminated sediments from the Gulf of California, Mexico, *Mar. Chem.*, *14*, 89–106, doi:10.1016/0304-4203(83)90072-5.

Byrne, J. V., and K. O. Emery (1960), Sediments of the Gulf of California, *Geol. Soc. Am. Bull.*, *71*, 983–1010, doi:10.1130/0016-7606(1960)71[983:SOTGOC]2.0.CO;2.

Calvert, S. E. (1964), Factors affecting distribution of laminated diatomaceous sediments in the Gulf of California, in *Marine Geology of the Gulf of California*, *Mem.*, vol. 3, edited by T. H. van Andel and G. G. Shor Jr., pp. 311–330, Am. Assoc. of Pet. Geol., Tulsa, Okla.

Calvert, S. E. (1966a), Accumulation of diatomaceous silica in the sediments of the Gulf of California, *Geol. Soc. Am. Bull.*, *77*, 569–596, doi:10.1130/0016-7606(1966)77[569:AODSIT]2.0.CO;2.

Calvert, S. E. (1966b), Origin of diatom-rich, varved sediments from the Gulf of California, *J. Geol.*, *74*, 546–565.

Calvert, S. E., and T. F. Pedersen (1996), Sedimentary geochemistry of manganese: Implications for the environment of formation of manganiferous black shales, *Econ. Geol.*, *91*, 36–47, doi:10.2113/gsecongeo.91.1.36.

Calvert, S. E., and T. F. Pedersen (2007), Elemental proxies for palaeoclimatic and palaeoceanographic variability in marine sediments: Interpretation and application, in *Paleoceanography of the Late Cenozoic. Part 1. Methods in Late Cenozoic Paleoceanography*, edited by C. Hillaire-Marcel and A. de Vernal, pp. 567–644, Elsevier, New York.

Cartapanis, O., K. Tachikawa, and E. Bard (2011), Northeastern Pacific oxygen minimum zone variability over the past 70 kyr: Impact of biological production and oceanic ventilation, *Paleoceanography*, *26*, PA4208, doi:10.1029/2011PA002126.

Chang, A. S., T. F. Pedersen, and I. L. Hendy (2008), Late Quaternary palaeoproductivity history on the Vancouver Island Margin, western Canada: A multiproxy geochemical study, *Can. J. Earth Sci.*, *45*, 1283–1297, doi:10.1139/E08-038.

©2015. American Geophysical Union. All Rights Reserved.

Chang, A. S., T. F. Pedersen, and I. L. Hendy (2014), Effects of productivity, glaciation, and ventilation on late Quaternary sedimentary redox and trace element accumulation on the Vancouver Island margin, western Canada, *Paleoceanography*, *29*, 730–746, doi:10.1002/2013PA002581.
Cheshire, H., and J. Thurow (2013), High-resolution migration history of the Subtropical High/Trade Wind system of the northeastern Pacific during the last ~55 years: Implications for glacial atmospheric reorganization, *Paleoceanography*, *28*, 319–333, doi:10.1002/palo.20031.
Cheshire, H., J. Thurow, and A. J. Nederbragt (2005), Late Quaternary climate change record from two long sediment cores from Guaymas Basin, Gulf of California, *J. Quat. Sci.*, *20*, 457–469, doi:10.1002/jqs.944.
Chikamoto, M. O., L. Menviel, A. Abe-Ouchi, R. Ohgaito, A. Timmerman, Y. Okazaki, N. Harada, and A. Oka (2012), Variability in North Pacific intermediate and deep water ventilation during Heinrich events in two coupled climate models, *Deep Sea Res., Part II*, *61*, 114–126, doi:10.1016/j.dsr2.2011.12.002.
Clement, A. C., and L. C. Peterson (2008), Mechanisms of abrupt climate change of the last glacial period, *Rev. Geophys.*, *46*, RG4002, doi:10.1029/2006RG000204.
Collier, R. W. (1985), Molybdenum in the northeast Pacific Ocean, *Limnol. Oceanogr.*, *30*, 1351–1354.
Colodner, D., J. Sachs, G. Ravizza, K. Turekian, J. Edmond, and E. Boyle (1993), The geochemical cycle of rhenium: A reconnaissance, *Earth Planet. Sci. Lett.*, *117*, 205–221, doi:10.1016/0012-821X(93)90127-U.
Crusius, J., S. Calvert, T. Pedersen, and D. Sage (1996), Rhenium and molybdenum in sediments as indicators of oxic, suboxic and sulfidic conditions of deposition, *Earth Planet. Sci. Lett.*, *145*, 65–78, doi:10.1016/S0012-821X(96)00204-X.
Crusius, J., T. F. Pedersen, S. E. Calvert, G. L. Cowie, and T. Oba (1999), A 36 kyr geochemical record from the Sea of Japan of organic matter flux variations and changes in intermediate water oxygen concentrations, *Paleoceanography*, *14*, 248–259, doi:10.1029/1998PA900023.
Cullen, J. T., and R. M. Sherrell (2005), Effects of dissolved carbon dioxide, zinc, and manganese on the cadmium to phosphorus ratio in natural phytoplankton assemblages, *Limnol. Oceanogr.*, *50*, 1193–1204.
Dansgaard, W., et al. (1993), Evidence for general instability of past climate from a 250 kyr ice-core record, *Nature*, *364*, 218–220, doi:10.1038/364218a0.
Dean, W. E. (2006), The geochemical record of the last 17,000 years in the Guaymas Basin, Gulf of California, *Chem. Geol.*, *232*, 87–98, doi:10.1016/j.chemgeo.2006.02.017.
Dean, W. E., C. Pride, and R. Thunell (2004), Geochemical cycles in sediments deposited on the slopes of the Guaymas and Carmen Basins of the Gulf of California over the last 180 years, *Quat. Sci. Rev.*, *23*, 1817–1833, doi:10.1016/j.quascirev.2004.03.010.
Dean, W. E., Y. Zheng, J. D. Ortiz, and A. van Geen (2006), Sediment Cd and Mo accumulation in the oxygen-minimum zone off western Baja California linked to global climate over the past 52 kyr, *Paleoceanography*, *21*, PA4209, doi:10.1029/2005PA001239.
Delgadillo-Hinojosa, F., J. V. Macías-Zamora, J. A. Segovia-Zavala, and S. Torres-Valdés (2001), Cadmium enrichment in the Gulf of California, *Mar. Chem.*, *75*, 109–122, doi:10.1016/S0304-4203(01)00028-7.
Doose, H., F. G. Prahl, and M. W. Lyle (1997), Biomarker temperature estimates for modern and last glacial surface waters of the California Current system between 33° and 42°N, *Paleoceanography*, *12*, 615–622, doi:10.1029/97PA00821.
Douglas, R., O. Gonzalez-Yajimovich, J. Ledesma-Vazquez, and F. Staines-Urias (2007), Climate forcing, primary production and the distribution of Holocene biogenic sediments in the Gulf of California, *Quat. Sci. Rev.*, *26*, 115–129, doi:10.1016/j.quascirev.2006.05.003.
Dyrssen, D., and K. Kremling (1990), Increasing hydrogen sulphide concentrations and trace metal behaviour in the anoxic Baltic waters, *Mar. Chem.*, *30*, 193–204, doi:10.1016/0304-4203(90)90070-S.
Galbraith, E. D., M. Kienast, S. L. Jaccard, T. F. Pedersen, B. G. Brundle, and T. Kiefer (2008), Consistent relationship between global climate and surface nitrate utilization in western subarctic Pacific throughout the last 500 kyr, *Paleoceanography*, *23*, PA2212, doi:10.1029/2007PA001518.
Ganeshram, R. S., and T. F. Pedersen (1998), Glacial-interglacial variability in upwelling and bioproductivity off NW Mexico: Implications for Quaternary paleoclimate, *Paleoceanography*, *13*, 634–645, doi:10.1029/98PA02508.
Garcia, H. E., R. A. Locarnini, T. P. Boyer, and J. I. Antonov (2006), *World Ocean Atlas 2005*, *Dissolved Oxygen, Apparent Oxygen Utilization, and Oxygen Saturation, NOAA Atlas NESDIS 63*, 342 pp., vol. 3, edited by S. Levitus, U.S. Gov. Print. Off., Washington, D. C.
Hartnett, H. E., and A. H. Devol (2003), Role of a strong oxygen-deficient zone in the preservation and degradation of organic matter: A carbon budget for the continental margins of northwest Mexico and Washington State, *Geochim. Cosmochim. Acta*, *67*(2), 247–264, doi:10.1016/S0016-7037(02)01076-1.
Helz, G. R., and M. K. Dolor (2012), What regulates rhenium in euxinic basins?, *Chem. Geol.*, *304–305*, 131–141, doi:10.1016/j.chemgeo.2012.02.011.
Helz, G. R., E. Bura-Nakic, N. Mikac, and I. Ciglenecki (2011), New model for molybdenum behavior in euxinic waters, *Chem. Geol.*, *284*(3–4), 323–332, doi:10.1016/j.chemgeo.2011.03.012.
Hendy, I. L., and T. F. Pedersen (2005), Is pore water oxygen content decoupled from productivity on the California margin? Trace element results from Ocean Drilling Program Hole 1017E, San Lucia Slope, California, *Paleoceanography*, *20*, PA4026, doi:10.1029/2004PA001123.
Hendy, I. L., T. F. Pedersen, J. P. Kennett, and R. Tada (2004), Intermittent existence of a southern Californian upwelling cell during submillennial climate change of the last 60 kyr, *Paleoceanography*, *19*, PA3007, doi:10.1029/2003PA000965.
Herbert, T. D., J. D. Schuffert, D. Andreasen, L. Heusser, M. Lyle, A. C. Mix, A. C. Ravelo, L. D. Stott, and J. C. Herguera (2001), The collapse of the California Current during glacial maxima linked to climate change on land, *Science*, *293*, 71–76, doi:10.1126/science.1059209.
Herguera, J. C., T. Herbert, M. Kashgarian, and C. Charles (2010), Intermediate and deep water mass distribution in the Pacific during the Last Glacial Maximum inferred from oxygen and carbon stable isotopes, *Quat. Sci. Rev.*, *29*(9–10), 1228–1245, doi:10.1016/j.quascirev.2010.02.009.
Hickey, B. M. (1979), The California Current system: Hypotheses and facts, *Prog. Oceanogr.*, *8*, 191–279, doi:10.1016/0079-6611(79)90002-8.
Hostetler, S. W., P. U. Clark, P. J. Bartlein, A. C. Mix, and N. J. Pisias (1999), Atmospheric transmission of North Atlantic Heinrich events, *J. Geophys. Res.*, *104*, 3947–3952, doi:10.1029/1998JD200067.
Ivanochko, T. S., and T. F. Pedersen (2004), Determining the influences of late Quaternary ventilation and productivity variations on Santa Barbara Basin sedimentary oxygenations: A multiproxy approach, *Quat. Sci. Rev.*, *23*, 467–480, doi:10.1016/j.quascirev.2003.06.006.
Kahru, M., S. G. Marinone, S. E. Lluch-Cota, A. Parés-Sierra, and B. G. Mitchell (2004), Ocean-color variability in the Gulf of California: Scales from days to ENSO, *Deep Sea Res., Part II*, *51*, 139–146, doi:10.1016/j.dsr2.2003.04.001.
Keigwin, L. D. (1998), Glacial-age hydrography of the far northwest Pacific Ocean, *Paleoceanography*, *13*, 323–339, doi:10.1029/98PA00874.
Keigwin, L. D. (2002), Late Pleistocene-Holocene paleoceanography and ventilation of the Gulf of California, *J. Oceanogr.*, *58*, 421–432, doi:10.1023/A:1015830313175.
Keigwin, L. D., and G. A. Jones (1990), Deglacial climatic oscillations in the Gulf of California, *Paleoceanography*, *5*, 1009–1023, doi:10.1029/PA005i006p01009.
Kelts, K., and J. Nimitz (1982), Preliminary sedimentology of late Quaternary diatomaceous muds from Deep Sea Drilling Project site 480, Guaymas Basin slope, Gulf of California, *Initial Rep. Deep Sea Drill. Proj.*, *64*, 1191–1210, doi:10.2973/dsdp.proc.64.159.1982.

©2015. American Geophysical Union. All Rights Reserved.

Kienast, S. S., S. E. Calvert, and T. F. Pedersen (2002), Nitrogen isotope and productivity variations along the northeast Pacific margin over the last 120 kyr: Surface and subsurface paleoceanography, *Paleoceanography*, *17*(4), 1055, doi:10.1029/2001PA000650.

Koide, M., V. F. Hodge, J. S. Yang, M. Stallard, E. G. Goldberg, J. Calhoun, and K. K. Bertine (1986), Some comparative marine chemistries of rhenium, gold, silver and molybdenum, *Appl. Geochem.*, *1*, 705–714.

Kramer, D., J. T. Cullen, J. R. Christian, W. K. Johnson, and T. F. Pedersen (2011), Silver in the subarctic northeast Pacific Ocean: Explaining the basin scale distribution of silver, *Mar. Chem.*, *123*, 133–142, doi:10.1016/j.marchem.2010.11.002.

Lane, T. W., and F. M. M. Morel (2000), A biological function for cadmium in marine diatoms, *Proc. Natl. Acad. Sci. U.S.A.*, *97*, 4627–4631, doi:10.1073/pnas.090091397.

Lee, J. G., S. B. Roberts, and F. M. M. Morel (1995), Cadmium: A nutrient for the marine diatom *Thalassiosira weissflogii*, *Limnol. Oceanogr.*, *40*, 1056–1063.

Li, Y.-H., and S. Gregory (1974), Diffusion of ions in sea water and in deep-sea sediments, *Geochim. Cosmochim. Acta*, *38*, 703–714, doi:10.1016/0016-7037(74)90145-8.

Lisiecki, L. E., and M. E. Raymo (2005), A Pliocene-Pleistocene stack of 57 globally distributed benthic δ^{18}O records, *Paleoceanography*, *20*, PA1003, doi:10.1029/2004PA001071.

Manheim, F. T. (1970), The diffusion of ions in unconsolidated sediments, *Earth Planet. Sci. Lett.*, *9*, 307–309, doi:10.1016/0012-821X(70)90123-8.

Masuzawa, T., S. Noriki, T. Kurosaki, S. Tsunogai, and M. Koyama (1989), Compositional change of settling particles with water depth in the Japan Sea, *Mar. Chem.*, *27*, 61–78, doi:10.1016/0304-4203(89)90028-5.

McClymont, E. L., R. Ganeshram, L. E. Pichevin, H. M. Talbot, B. E. van Dongen, R. C. Thunell, A. M. Haywood, J. S. Singarayer, and P. J. Valdes (2012), Sea-surface temperature records of Termination 1 in the Gulf of California: Challenges for seasonal and inter-annual analogues of tropical Pacific climate change, *Paleoceanography*, *27*, PA2202, doi:10.1029/2011PA002226.

McKay, J. L., and T. F. Pedersen (2008), The accumulation of silver in marine sediment: A link to biogenic Ba and marine productivity, *Global Biogeochem. Cycles*, *22*, GB4010, doi:10.1029/2007GB003136.

McLennan, S. M. (2001), Relationships between the trace element composition of sedimentary rocks and upper continental crust, *Geochem. Geophys. Geosyst.*, *2*(4), 1021, doi:10.1029/2000GC000109.

Morford, J. L., S. R. Emerson, E. J. Breckel, and S. H. Kim (2005), Diagenesis of oxyanions (V, U, Re, and Mo) in pore waters and sediments from a continental margin, *Geochim. Cosmochim. Acta*, *69*, 5021–5032, doi:10.1016/j.gca.2005.05.015.

Morford, J. L., W. R. Martin, R. Francois, and C. M. Carney (2009), A model for uranium, rhenium, and molybdenum diagenesis in marine sediments based on results from coastal locations, *Geochim. Cosmochim. Acta*, *73*(10), 2938–2960, doi:10.1016/j.gca.2009.02.029.

Morford, J. L., W. R. Martin, and C. M. Carney (2012), Rhenium geochemical cycling: Insights from continental margins, *Chem. Geol.*, *324–325*, 73–86, doi:10.1016/j.chemgeo.2011.12.014.

Mortlock, R. A., and P. N. Froelich (1989), A simple method for the rapid determination of biogenic opal in pelagic marine sediments, *Deep Sea Res.*, *36*, 1415–1426, doi:10.1016/0198-0149(89)90092-7.

Nameroff, T. J., L. S. Balistrieri, and J. W. Murray (2002), Suboxic trace metal geochemistry in the eastern tropical North Pacific, *Geochim. Cosmochim. Acta*, *66*(7), 1139–1158, doi:10.1016/S0016-7037(01)00843-2.

Nameroff, T. J., S. E. Calvert, and J. W. Murray (2004), Glacial-interglacial variability in the eastern tropical North Pacific oxygen minimum zone recorded by redox-sensitive trace metals, *Paleoceanography*, *19*, PA1010, doi:10.1029/2003PA000912.

Pichevin, L. E., R. S. Ganeshram, B. C. Reynolds, F. Prahl, T. F. Pedersen, R. Thunell, and E. L. McClymont (2012), Silicic acid biogeochemistry in the Gulf of California: Insights from sedimentary Si isotopes, *Paleoceanography*, *27*, PA2201, doi:10.1029/2011PA002237.

Pichevin, L. E., R. S. Ganeshram, W. Giebert, R. Thunell, and R. Hinton (2014), Silica burial enhanced by iron limitation in oceanic upwelling margins, *Nat. Geosci.*, *7*, 541–546, doi:10.1038/ngeo2181.

Pike, J., and A. E. S. Kemp (1996), Records of seasonal flux in Holocene laminated sediments, Gulf of California, in *Palaeoclimatology and Palaeoceanography from Laminated Sediments*, edited by A. E. S. Kemp, *Geol. Soc. London Spec. Publ.*, *116*, pp. 157–169, doi:10.1144/GSL.SP.1996.116.01.14.

Price, A. M., K. N. Mertens, V. Pospelova, T. F. Pedersen, and R. S. Ganeshram (2013), Late Quaternary climatic and oceanographic changes in the northeast Pacific as recorded by dinoflagellate cysts from Guaymas Basin, Gulf of California, *Paleoceanography*, *28*, 200–212, doi:10.1002/palo.20019.

Pride, C., R. Thunell, D. Sigman, L. Keigwin, M. Altabet, and E. Tappa (1999), Nitrogen isotopic variations in the Gulf of California since the last deglaciation: Response to global climate change, *Paleoceanography*, *14*, 397–409, doi:10.1029/1999PA900004.

Rau, G. H., R. E. Sweeney, and I. R. Kaplan (1982), Plankton ^{13}C:^{12}C ratio changes with latitude: Differences between northern and southern oceans, *Deep Sea Res., Part A*, *29*, 1035–1039, doi:10.1016/0198-0149(82)90026-7.

Reinfelder, J. R., and N. S. Fisher (1991), The assimilation of elements ingested by marine copepods, *Science*, *251*, 794–796, doi:10.1126/science.251.4995.794.

Romanova, V., G. Lohmann, K. Grosfeld, and M. Butzin (2006), The relative role of oceanic heat transport and orography on glacial climate, *Quat. Sci. Rev.*, *25*(7–8), 832–845, doi:10.1016/j.quascirev.2005.07.007.

Rosenthal, Y., P. Lam, E. A. Boyle, and J. Thomson (1995), Authigenic cadmium enrichments in suboxic sediments: Precipitation and postdepositional mobility, *Earth Planet. Sci. Lett.*, *132*, 99–111, doi:10.1016/0012-821X(95)00056-I.

Sancetta, C. (1995), Diatoms in the Gulf of California: Seasonal flux patterns and the sediment record for the last 15,000 years, *Paleoceanography*, *10*, 67–84, doi:10.1029/94PA02796.

Schmittner, A., E. D. Galbraith, S. W. Hostetler, T. F. Pedersen, and R. Zhang (2007), Large fluctuations of dissolved oxygen in the Indian and Pacific Oceans during Dansgaard-Oeschger oscillations caused by variations of North Atlantic Deep Water subduction, *Paleoceanography*, *22*, PA3207, doi:10.1029/2006PA001384.

Segovia-Zavala, J. A., F. Delgadillo-Hinojosa, M. L. Lares-Reyes, M. A. Huerta-Díaz, A. Munoz-Barbosa, and E. V. Torres-Delgado (2009), Atmospheric input and concentration of dissolved iron in the surface layer of the Gulf of California, *Cienc. Mar.*, *35*, 75–90.

Segovia-Zavala, J. A., M. L. Lares, F. Delgadillo-Hinojosa, A. Tovar-Sánchez, and S. A. Sañudo-Wilhelmy (2010), Dissolved iron distributions in the central region of the Gulf of California, Mexico, *Deep Sea Res., Part I*, *57*, 53–64, doi:10.1016/j.dsr.2009.10.007.

Shimmield, G. B., and N. B. Price (1986), The behavior of molybdenum and manganese during early sediment diagenesis offshore Baja California, Mexico, *Mar. Chem.*, *19*, 261–280, doi:10.1016/0304-4203(86)90027-7.

Sigman, D. M., M. A. Altabet, R. H. Michener, D. C. McCorkle, B. Fry, and R. M. Holmes (1997), Natural abundance-level measurement of the nitrogen isotopic composition of oceanic nitrate: An adaption of the ammonia diffusion method, *Mar. Chem.*, *57*, 227–242, doi:10.1016/S0304-4203(97)00009-1.

Singh, S. P., S. K. Singh, and R. Bhushan (2011), Behavior of redox sensitive elements (U, Mo and Re) in the water column of the Bay of Bengal, *Mar. Chem.*, *126*, 76–88, doi:10.1016/j.marchem.2011.04.001.

©2015. American Geophysical Union. All Rights Reserved.

Sohrin, Y., K. Isshiki, and T. Kuwamoto (1987), Tungsten in North Pacific waters, *Mar. Chem.*, *22*, 95–103, doi:10.1016/0304-4203(87)90051-X.
Stuiver, M., and P. Grootes (2000), GISP2 oxygen isotope ratios, *Quat. Res.*, *53*, 277–284, doi:10.1006/qres.2000.2127.
Takahashi, K. (1998), The Bering and Okhotsk Seas: Modern and past paleoceanographic changes and gateway impact, *J. Asian Earth Sci.*, *16*, 49–58, doi:10.1016/S0743-9547(97)00048-2.
Talley, L. D. (1991), An Okhotsk Sea water anomaly: Implications for ventilation in the North Pacific, *Deep Sea Res., Part A*, *38*, S171–S190.
Thomson, R. E., and M. V. Krassovski (2010), Poleward reach of the California Undercurrent extension, *J. Geophys. Res.*, *115*, C09027, doi:10.1029/2010JC006280.
Thunell, R. C. (1998), Seasonal and annual variability in particle fluxes in the Gulf of California: A response to climate forcing, *Deep Sea Res., Part I*, *45*, 2059–2083, doi:10.1016/S0967-0637(98)00053-3.
Thunell, R. C., C. J. Pride, E. Tappa, and F. E. Muller-Karger (1993), Varve formation in the Gulf of California: Insights from time series sediment trap sampling and remote sensing, *Quat. Sci. Rev.*, *12*, 451–464, doi:10.1016/S0277-3791(05)80009-5.
Thunell, R. C., C. J. Pride, E. Tappa, and F. E. Muller-Karger (1994), Biogenic silica fluxes and accumulation rates in the Gulf of California, *Geology*, *22*, 303–306, doi:10.1130/0091-7613(1994)022<0303:BSFAAR>2.3.CO;2.
Thunell, R. C., C. J. Pride, P. Ziveri, F. Muller-Karger, C. Sancetta, and D. Murray (1996), Plankton response to physical forcing in the Gulf of California, *J. Plankton Res.*, *18*, 2017–2026, doi:10.1093/plankt/18.11.2017.
Tribovillard, N., T. J. Algeo, T. Lyons, and A. Riboulleau (2006), Trace metals as paleoredox and palaeoproductivity proxies: An update, *Chem. Geol.*, *232*(1–2), 12–32, doi:10.1016/j.chemgeo.2006.02.012.
van Geen, A., D. C. McCorkle, and G. P. Klinkhammer (1995), Sensitivity of the phosphate-cadmium-carbon isotope relation in the ocean to cadmium removal by suboxic sediments, *Paleoceanography*, *10*, 159–169, doi:10.1029/94PA03352.
van Geen, A., Y. Zheng, J. M. Bernhard, K. G. Cannariato, J. Carriquiry, W. E. Dean, B. W. Eakins, J. D. Ortiz, and J. Pike (2003), On the preservation of laminated sediments along the western margin of North America, *Paleoceanography*, *18*(4), 1098, doi:10.1029/2003PA000911.
Van Scoy, K. A., D. B. Olson, and R. A. Fine (1991), Ventilation in the North Pacific intermediate waters: The role of the Alaskan Gyre, *J. Geophys. Res.*, *96*, 16,801–16,810, doi:10.1029/91JC01783.
Wagner, M., I. L. Hendy, J. L. McKay, and T. F. Pedersen (2013), Influence of biological productivity on silver and redox-sensitive trace metal accumulation in Southern Ocean surface sediments, Pacific sector, *Earth Planet. Sci. Lett.*, *380*, 31–40, doi:10.1016/j.epsl.2013.08.020.
Wyrtki, K. (1962), The oxygen minima in relation to ocean circulation, *Deep Sea Res. Oceanogr. Abstr.*, *9*, 11–23, doi:10.1016/0011-7471(62)90243-7.
Xu, Y., and W.-X. Wang (2004), Silver uptake by a marine diatom and its transfer to the coastal copepod *Acartia spinicauda*, *Environ. Toxicol. Chem.*, *23*, 682–690, doi:10.1897/1551-5028(2004)023<0682:SUBAMD>2.0.CO;2.
Zhang, Y., H. Obata, and Y. Nozaki (2004), Silver in the Pacific Ocean and the Bering Sea, *Geochem. J.*, *38*, 623–633.
Zheng, Y., A. van Geen, R. F. Anderson, J. V. Gardner, and W. E. Dean (2000), Intensification of the northeast Pacific oxygen minimum zone during the Bølling-Allerød warm period, *Paleoceanography*, *15*, 528–536, doi:10.1029/1999PA000473.

©2015. American Geophysical Union. All Rights Reserved.